Surface albedo as a proxy for land-cover clearing in seasonally dry forests: Evidence from the Brazilian Caatinga

John Cunha[a,*], Rodolfo L. B. Nóbrega[c,d] , Iana Rufino[b], Stefan Erasmi[e], Carlos Galvao[b], Fernanda Valente[f]

[Updated version: 29 May 2019]

[a]Federal University of Campina Grande, Centre for the Sustainable Development of the Semi - Arid, Sumé, Brazil;
[b]Federal University of Campina Grande, Centre for Natural Resources and Technology, Campina Grande, Brazil;
[c]University of Reading, School of Archaeology, Geography and Environmental Science, Reading, United Kingdom;
[d]Imperial College London, Faculty of Natural Sciences, Department of Life Sciences, Ascot, United Kingdom;
[e]University of Goettingen, Institute of Geography, Cartography GIS & Remote Sensing Section, Goettingen, Germany;
[f]University of Lisbon, School of Agriculture, Forest Research Centre (CEF), Tapada da Ajuda, 1349-017 Lisbon, Portugal.
[*]Corresponding author: john.brito@ufcg.edu.br

Abstract:

Ongoing increase in human and climate pressures, in addition to the lack of monitoring initiatives, make the Caatinga one of the most vulnerable forests in the world. The Caatinga is located in the semi-arid region of Brazil and its vegetation phenology is highly dependent on precipitation, which has a high spatial and temporal variability. Under these circumstances, satellite image-based methods are valued due to their ability to uncover human-induced changes from climate effects on land cover. In this study, a time series stack of 670 Landsat images over a period of 31 years (1985–2015) was used to investigate spatial and temporal patterns of land-cover clearing (LCC) due to vegetation removal in an area of the Caatinga. We compared the LCC detection accuracy of three spectral indices, i.e., the surface albedo (SA), the Enhanced Vegetation Index (EVI) and the Normalized Difference Vegetation Index (NDVI). We applied a residual trend analysis (TSS-RESTREND) to attenuate seasonal climate effects on the vegetation time series signal and to detect only significant

structural changes (breakpoints) from monthly Landsat time series. Our results show that SA was able to identify the general occurrence of LCC and the year that it occurred with a higher accuracy (89 and 62%, respectively) compared to EVI (44 and 22%) and NDVI (46 and 22%). The overall outcome of the study shows the benefits of using Landsat time series and a spectral index that incorporates the short-wave infrared range, such as the SA, compared to visible and near-infrared vegetation indices for monitoring LCC in seasonally dry forests such as the Caatinga.
Keywords: vegetation index; time series; Landsat; land-cover change; semi-arid climate.

1. Introduction

The identification of land-cover alteration driven by human action is one of the main challenges when studying seasonally dry forests (Yang et al., 2016; Wessels et al., 2007), as it is difficult to differentiate forest from non-forest areas (Mayes et al., 2015). In these areas, vegetation greenness is strongly related to the annual precipitation averages as well as the spatial variability and shifts of the rainy season period within a year (Hein et al., 2011). This effect of temporal and spatial climatic variability often masks the human actions in seasonally dry forests, especially after long drought periods (Zhang et al., 2014), because the dry vegetation sustains an extremely low level of photosynthetic material (Jacques et al., 2014), which is usually used as an indicator of changes in land cover of forests (Eckert et al., 2015; Tucker 1979; Xu et al., 2014). However, even under these circumstances, forests lose a very large proportion of the aboveground biomass when they are cleared (IPCC, 2000). The identification of changes in terrestrial forest biomass on an annual basis is a prerequisite for improving estimates of terrestrial water, energy, and carbon sources

and exchanges (Le Toan et al., 2011; Steyaert and Knox, 2008). Such assessment is possible with time-series analysis, which is a widely accepted method to identify vegetation clearing (Gómez et al., 2016; Song et al., 2014).

Long time series of satellite data are suitable to assess vegetation dynamics on regional scales (Schucknecht et al., 2013). In this context, Landsat data is one of the most valuable sources of global observation. Owing to more than 30 years of medium-resolution and multispectral data, Landsat datasets constitute the longest continuous remotely-sensed record of the Earth's surface (Loveland and Dwyer, 2012). Despite its low temporal resolution at 16 days, earlier problems in geometric accuracy (Dwyer et al., 2018), and necessary adjustments of bidirectional reflectance effects (Egorov et al., 2018), Landsat imagery quality has improved. Landsat dataset structure provides information on radiometric, geometric and cloud cover quality to support temporal analysis (Wulder et al., 2016). The higher-level products are freely available through the United States Geological Survey (USGS) and allow users to retrieve surface reflectance data (Ju and Masek, 2016).

Trend analysis of indices based on visible and near-infrared (VIS–NIR wavelength ranges (0.4–1.1 μm) and computed from multi-year satellite data has been widely and successfully used to monitor changes in vegetation productivity (Fensholt et al., 2012; Higginbottom and Symeonakis, 2014; De Jong et al., 2012) and land degradation (Li et al., 2016; Mariano et al., 2018). Although the trade-offs between land-cover clearing (LCC) and climate are well-documented, LCC analyses also need to consider the climate and vegetation background of a particular region (Liu et al., 2016; Schwinning et al., 2004). The detection of LCC in seasonally dry forests by using VIS–NIR, such as EVI and NDVI, is limited due to difficulties distinguishing deciduous vegetation from the underlying ground during the dry period (Daughtry, 2001; Jacques

et al., 2014; Mayes et al., 2015; Nagler et al., 2000; Xu et al., 2014). Zhao et al. (2018) highlight that while vegetation indices are routinely used to monitor ecosystem attributes and functions such as vegetation cover and primary productivity, the remote sensing-measured surface albedo (SA) can be used to assess ecosystem status in drylands. SA is more sensitive to changes in biomass (Rodríguez-Caballero et al., 2015); it has been used to monitor changes in dryland ecosystems because SA increases as soils become more exposed to direct sunlight (Yu et al., 2017), which is the first outcome of the LCC process on the terrestrial surface (Lamchin et al., 2016; Liu et al., 2016; Karnieli et al., 2014). SA is also reported to be sensitive to seasonal phenological variations (Samain et al., 2008; Wang et al., 2017), which are caused primarily by climatic variability in dry forests.

Different statistical approaches based on satellite data have been used to distinguish the effects of climatic variability on vegetation from anthropogenic actions on land cover in seasonally dry forests (Anyamba et al., 2014; DeVries et al., 2015; Evans and Geerken, 2004; Higginbottom and Symeonakis, 2014; Ibrahim et al., 2015; Karlson and Ostwald, 2016; Leroux et al., 2017; Verbesselt et al., 2016). In most of these studies, changes in the environment are identified by using trend analysis methods that remove the seasonal cycle within the time series. Here, we highlight two of them, considering their effectiveness to detect LCC in seasonally dry forests: the RESidual TREND (RESTREND, Evans and Geerken, 2004; Li et al., 2016; Wessels et al., 2012) and the Break detection For Additive Season and Trend (BFAST, DeVries et al., 2015; Dutrieux et al., 2015; Verbesselt et al., 2012) methods. The RESTREND method is capable of coping with inter-annual rainfall variability and trends for detection of realistic levels of human-induced LCC by considering the residuals of the regression between the target variable (e.g., NDVI) and rainfall (Wessels et al., 2012). The BFAST

111 method decomposes the time series for detecting structural changes in both the trend
112 and seasonal components to identify changes in land cover (De Jong et al., 2012). The
113 TSS-RESTREND (Time Series Segmentation and RESidual TREND) method (Burrell
114 et al., 2017) combines the RESTREND and BFAST analyses in order to attenuate
115 seasonal climate effects and to detect structural changes (breakpoints). Further, TSS-
116 RESTREND adds the Chow test (Chow, 1960) to identify the most significant
117 breakpoint in the time series. The Chow test and the representation of the seasonal
118 component by RESTREND are relevant mechanisms in TSS-RESTREND to overcome
119 the limitations of the RESTREND and BFAST methods when each method is applied
120 alone. The TSS-RESTREND method can be divided into two main components, one
121 for a structural change (breakpoint) detection and the other for an overall trend
122 estimation. While the first one is feasible to detect changes that occur abruptly, such
123 as LCC, the latter is suitable to identify trends that happen over a longer period of time.
124 In our study, we focus on the use of the structural change detection component
125 of the TSS-RESTREND method in the Caatinga, which is a seasonally dry forest
126 constrained by climatic and anthropogenic pressures. Located in Northeastern Brazil,
127 a region dominated by a semi-arid climate with high temporal and spatial rainfall
128 variability (Marengo et al., 2017), the Caatinga vegetation is a heterogeneous (Rodal
129 et al., 2008), seasonally dry forest (Albuquerque et al., 2012; Brito et al., 2012), with
130 its phenology driven by short-term rainfall patterns (Erasmi et al., 2014; Lima and
131 Rodal, 2010). In this region, the natural land cover has been cleared by anthropogenic
132 actions, which typically occur at small spatial scales and can thus be better identified
133 by using high spatial resolution observations (Lambin et al., 2003; Munyati et al., 2013;
134 Stroppiana et al., 2012). However, most vegetation studies that analyse long (> 30

years) remote sensing time series use vegetation indices at low spatial resolution, i.e., 1 to 8 km (Leroux et al., 2017).

Our hypothesis is that SA is a better indicator for LCC detection in seasonally dry forests, such as the Caatinga, compared to VIS–NIR vegetation indices, here represented by EVI and NDVI. Although SA is known to exhibit different responses between vegetated and bare soil surfaces, its use to identify or monitor LCC in dry forests has been poorly documented. We ascribe this scientific gap to the lack of global time-series datasets that provide multispectral data and to only recent developments on trend detection methods that translate the concept of abrupt LCC. In this study, this is addressed by applying the structural change component of the TSS-RESTREND method to a 31-year Landsat monthly time series to detect LCC in a seasonally dry forest in Northeastern Brazil (Caatinga) that has been threatened by LCC and fragmentation over the past decades.

2. Study area and data

2.1. Study area

The study area is located in the Brazilian Caatinga, a seasonally tropical dry forest that lies in Northeastern Brazil (Fig. 1A). Unlike most seasonally dry tropical forests that occur in isolated spots, the Caatinga spreads over a vast contiguous area, occupying ca. 910,000 km^2 as the largest continuous seasonally dry tropical forest and woodland vegetation (SDTFW) in the Americas (CNUC, 2017; Linares-Palomino et al., 2011). Although it is a unique ecosystem with a high degree of biodiversity and number of endemic species (Sobrinho et al., 2016), only 7.7% of its area is under environmental protection by the Brazilian National System of Conservation Units, which is 1.3% of restricted protection areas plus 6.4% of sustainable use areas (CNUC, 2017). The

Caatinga is considered the most neglected and threatened Brazilian major ecosystem due to inadequate and unsustainable use of its natural resources over the past decades (Moro et al., 2016). Native vegetated areas of the Caatinga have been cleared mainly because of ill-planned land use, which is directly influenced by how the land is used for living (Andrade-Silva et al., 2012; Araújo et al., 2007, 2010; Santos and Tabarelli, 2002). In our study area, like many other parts of the Caatinga, this has been commonly characterized by LCC caused by wood removal for firewood/charcoal production (Leal et al., 2005; Sobrinho et al., 2016). Reforestation initiatives are rare in the Caatinga and recuperation of the its vegetation in cleared areas is a challenge because it may take several decades to naturally re-establish the original land cover (Araújo et al., 2007; Lima et al., 2016; Pereira et al., 2003).

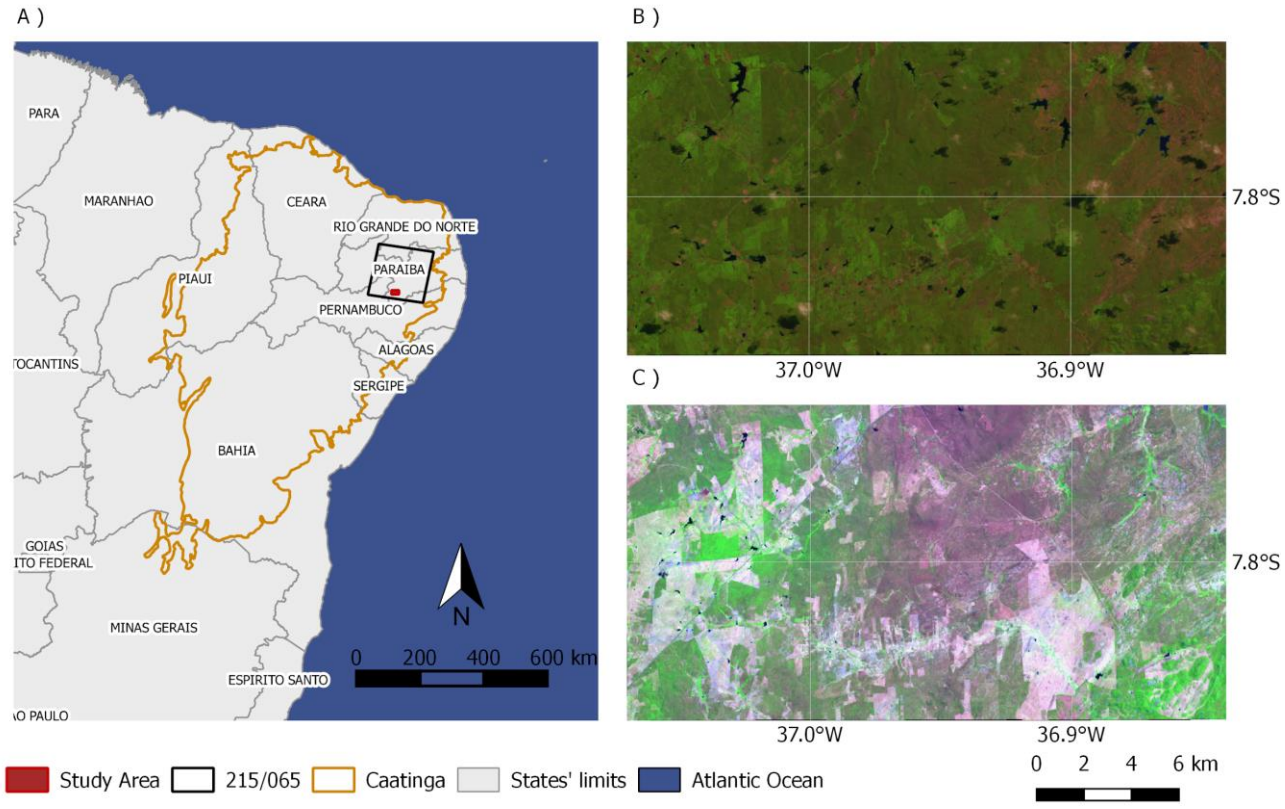

Fig. 1 - (A) Location of the Caatinga forest, Landsat scene 215/065 (path/row) and study area (Xmin: 37.07ºW; Xmax: 36.84ºW; Ymin: 7.86ºS; Ymax: 7.74ºS, WGS 84); (B) Landsat 5 false colour composite (RGB to bands 4, 3 and 2) of the study area on 17/06/1984; (C) Landsat 8 false colour composite (RGB

to bands 5, 4 and 3) of the same area of (B) on 06/05/2015, showing land-cover differences between the first and last years of the studied period.

Our area of study is part of the *Depressão Sertaneja Meridional* ecoregion of the Caatinga, which is the largest of Caatinga's eight ecoregions, occupying ca. 45% of the entire Caatinga and considered to have the most typical Caatinga phytogeographic distribution (Andrade-Lima, 1981; Velloso et al., 2001; Moro et al., 2016). The region where our study area is located, known as *Cariris Velhos*, was selected and used for decades for studies on hydrology and soil conservation due to its representativeness of the climate, soil, geology, vegetation and topography for the Brazilian semiarid/Caatinga region (Cadier, 1996; Nouvelot, 1974; Padilha et al., 2016). This region is also included in one of the Caatinga's desertification nuclei, which emphasize the application and need of our study there (Perez-Marin et al., 2012). In this area, the main economic activities are livestock and subsistence farming (Belchior et al., 2017), leading to substantial LCC (Fig. 1B and C). The climate is hot semi-arid (BSh, Köppen classification) (Alvares et al., 2013), with only two distinct seasons: the very hot rainy season (from February to May) and the hot dry season (from June to January). The average annual rainfall in this region is approximately 550 mm, with high interannual variability (coefficient of variation of approximately 30%) and an average annual temperature of 23°C (station code: 82792, INMET, 2018). The Standard Precipitation-Evapotranspiration Index (SPEI, Vicente-Serrano et al., 2010) for 12-month periods and the annual precipitation for the studied period and area shows that the alternation between dry and wet periods have different magnitudes over the studied years (Fig. 2). SPEI is a drought index based on the difference between precipitation and evapotranspiration that is often used to detect and monitor drought periods.

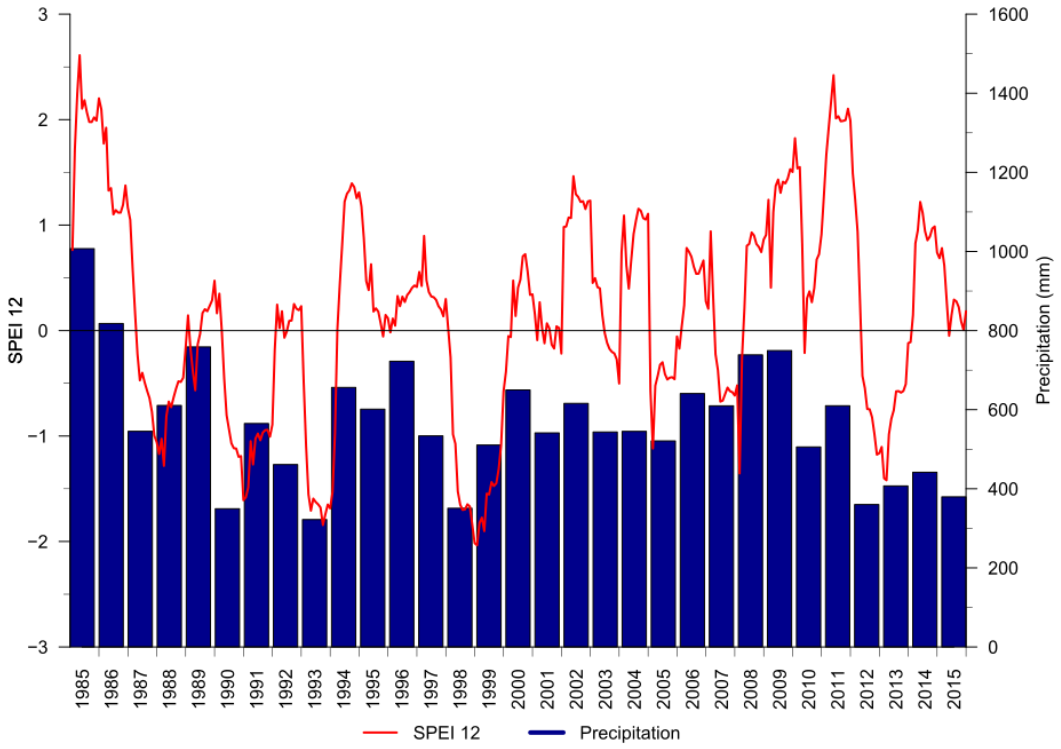

Fig. 2 - The 12-month Standardized Precipitation-Evapotranspiration Index - SPEI 12 (source: Beguería et al., 2017) and CHIRPS Precipitation (source: Funk et al., 2015) at geographic coordinates 36.75º W, 7.75º S (WGS 84).

2.2. Datasets

2.2.1. Landsat Surface Reflectance and Spectral Indices

In this study, we used the atmospherically corrected surface reflectance (SR) from the Landsat satellites that are freely available by the United States Geological Survey (https://espa.cr.usgs.gov/). SR data are generated at 30-meter spatial resolution every 16 days. USGS provides the standard processing of SR including the Level 1 Standard Terrain Correction, resulting in orthorectified images of high geometric accuracy. Two different algorithms generate the SR data depending on the sensor: for Landsat 5 TM and Landsat 7 ETM+ the SR data are obtained by the

LEDAPS software (Masek et al., 2006), and for Landsat 8 OLI data are processed by the LaSRC algorithm (Vermote et al., 2016).

We identified 670 available Landsat images from 1985 to 2015 that cover our study area (390 from TM, 233 from ETM+ and 47 from OLI). For our analysis we used the Landsat Surface Reflectance Quality Assessment (pixel_qa band) to consider only clear pixels (values 66 and 130 for Landsat 5 and 7, or 322 and 386 for Landsat 8, USGS, 2018a,b), which represented in average 307 clear acquisitions per grid cell for the 31-year time series.

For each Landsat image, NDVI (Tucker, 1979), EVI (Huete et al., 1997; 2002) and SA (Shuai et al., 2014, Wang et al., 2016) were calculated using Eqs. (1) to (3).

$$NDVI = \frac{\rho_{NIR} - \rho_{RED}}{\rho_{NIR} + \rho_{RED}} \quad (1)$$

$$EVI = 2.5 \times \frac{\rho_{NIR} - \rho_{RED}}{\rho_{NIR} + 6 \times \rho_{RED} - 7.5 \times \rho_{BLUE} + 1} \quad (2)$$

$$SA = b_{BLUE} \times \rho_{BLUE} + b_{GREEN} \times \rho_{GREEN} + b_{RED} \times \rho_{RED} + b_{NIR} \times \rho_{NIR} + b_{SWIR1} \times \rho_{SWIR1} + b_{SWIR2} \times \rho_{SWIR2} + b_0 \quad (3)$$

where ρ and b are the surface bidirectional reflectance values and their corresponding conversion coefficients for the six non-thermal Landsat bands, i.e., blue, green, red, NIR and the two shortwave infrared bands (SWIR1 and SWIR2). Table 1 shows the b values of the spectral bands of the three satellites used in this study. The highest values of the vegetation indices are found in vegetated areas, while the lowest values occur in areas of bare soil (Mariano et al., 2018; Rodríguez-Caballero et al., 2015; Zhao et al., 2018). As SA has an inverse behaviour to most VIS–NIR vegetation indices, we used its complement to one (1 - SA), thus ensuring a pattern of responses to LCC that corresponds to that of the vegetation indices EVI and NDVI.

Table 1 - Band conversion coefficients used to calculate shortwave albedo for the different Landsat data.

Sensor	b_{BLUE}	b_{GREEN}	b_{RED}	b_{NIR}	b_{SWIR1}	b_{SWIR2}	b_0
Landsat-5 TM	0.3206	0	0.1572	0.3666	0.1162	0.0457	- 0.0063
Landsat-7 ETM+	0.3141	0	0.1607	0.3694	0.1160	0.0456	- 0.0057
Landsat-8 OLI	0.2453	0.0508	0.1804	0.3081	0.1332	0.0521	0.0011

Flood (2013) showed that the medoid (a multi-dimensional analogue of the median) is a reliable measure to produce representative temporal image composites. In this study, we used the median to reduce the initial time series (SA, EVI and NDVI) to monthly composite images. Missing values were gap-filled by linear interpolation. Further, a linear Savitzky–Golay filter was applied (Cao et al., 2018; Chen et al., 2004; Savitzky and Golay, 1964), with a five-month half-width smoothing window in order to reduce the noise caused by atmospheric variability. The gap filling outcome is shown in the Supplementary material (Table S1 and Figs. S1 to S5).

2.2.2. Precipitation

The precipitation data used in this work were obtained from the Climate Hazards group InfraRed Precipitation with Stations (CHIRPS) dataset (Funk et al., 2015; Katsanos et al., 2016). CHIRPS is a near-global, very high spatial resolution (0.05° grid) precipitation product developed for monitoring environmental changes over land (Funk et al., 2015), which exhibited correlations ranging from 0.87 to 0.93 with rain gauge observations in the Caatinga (Paredes-Trejo et al., 2017). We used monthly precipitation data from October 1983 to December 2015.

3. Methods

3.1. TSS-RESTREND

The TSS-RESTREND method proposed by Burrell et al. (2017), combines the RESTREND technique (Evans and Geerken, 2004) and the BFAST methodology (Verbesselt et al., 2012, 2010), allowing a better and more accurate detection of structural changes in ecosystems. Prior to the application of trend analysis, it is frequently necessary to remove the influence of exogenous random factors (e.g., rainfall or temperature) that, in addition to time and space, has a considerable effect on the response variable. The removal process, either by parametric (e.g., regression) or nonparametric (e.g., LOWESS) methods, reduces the variability of the studied variable and increases the power to detect changes in it (Helsel and Hirsch, 2002; Schertz et al., 1991). In remote sensing, a similar procedure has been applied for land-cover analysis. The RESTREND method analyses the temporal trends in the vegetation precipitation relationship (VPR) residuals from a linear regression of the NDVI on the accumulated precipitation along a time period (Evans and Geerken, 2004).

In Burrell et al. (2017), VPR is obtained for two sets of information: complete NDVI time series (CTS-NDVI) and annual maximum NDVI. In both cases, the linear regression uses the Optimal Precipitation Accumulated (OPA) calculated on a per-pixel basis by an exhaustive search algorithm, which combines different accumulation periods and lag times. In our study, the OPA uses the CHIRPS precipitation data for accumulation periods of 1–12 months and lag times of 0–3 months, resulting in an increase of 15 months at the beginning of the precipitation series. The optimum VPR

274 is established by finding the highest correlation coefficients between OPA and CTS-
275 NDVI and between OPA and annual maximum NDVI.

276 In the structural change detection component of the TSS-RESTREND, the VPR
277 residuals are calculated for all pixels using the RESTREND method, and then applied
278 to the BFAST method (Verbesselt et al., 2010). The application of the BFAST returns
279 a list of breakpoints that are subsequently analysed by the Chow test (Chow, 1960).
280 The significance of each identified change is calculated and the most significant
281 breakpoint, if it exists, is selected as the structural change. More details on the TSS-
282 RESTREND method can be found in Burrell et al. (2017; 2018). In our study, we used
283 the TSS.RESTREND package (Burrell et al., 2017) for the R software environment (R
284 Core Team, 2017). Although this method was initially used with NDVI data (Burrell et
285 al., 2017), we additionally applied it to SA and EVI.

286 3.2. Verification Methodology

287 The performance of the TSS-RESTREND method was evaluated at both,
288 temporal and spatial levels. For each of the selected spectral indices and each pixel,
289 the year of the most significant breakpoint was registered and compared with the actual
290 LCC year in order to evaluate the performance of SA, EVI and NDVI. The actual (true)
291 year of LCC was determined by visual analysis of RapidEye images from 2015, which
292 are freely available for academic use through the Brazilian Ministry of the Environment
293 (MMA, 2018), Landsat images (false colour composite) and satellite data from Google
294 Earth Pro (Google, 2018).

295 The validation dataset used in this work was built using a two-step procedure.
296 First, a detailed visual survey of RapidEye images from 2015 allowed the identification
297 of several target areas where the original land cover had changed by the complete

298 removal of the vegetation. Then, Landsat images and Google Earth Pro imagery were
299 examined to determine the exact year of the LCC. Both products provided at least one
300 cloud-free composite image per year for the study period and area at the altitude of
301 visualization of 20 km. Additionally, several places that had no visible human impact
302 and that kept their original vegetation cover were also chosen as validation pixels. In
303 October 2017, field visits to the study area were conducted to confirm the land-cover
304 status. Three different types of areas were included in the validation dataset (Fig. 3):
305 1) 45 target areas of 120 m buffer each (ca. 80 pixels), from which 31 exhibit LCC in
306 the period 1985–2015 and 14 show a preserved natural vegetation; 2) a small region
307 of 4.5 km^2 that has undergone a well-delimited time-space LCC process over the
308 2003–2012 period, hereafter referred to as "Subset I"; and 3) a region of 42 km^2 that
309 has undergone a LCC process during 1985–2015, hereafter referred to as "Subset II".
310 The aerial median of each spectral index was calculated for each one of the 45
311 target areas. The TSS-RESTREND was then applied to the new generated time series.
312 Only the results from the structural change detection component of the TSS-
313 RESTREND were kept, namely the number of breakpoints, and the date and
314 respective confidence interval for the most significant breakpoint (hereafter referred to
315 as detected LCC year). Based on the statistical theory proposed by Bai (1997), the
316 breakpoints analysis implemented in the BFAST module (Verbesselt et al., 2010,
317 Zeileis et al., 2002) calculates confidence intervals for the change-point date with less
318 restrictive assumptions than those required by the usual parametric methods (i.e.,
319 independent and homogeneous normal errors). Due to these characteristics, these
320 intervals were used in the validation of our results. The output of the TSS-RESTREND
321 method was compared with the actual year of LCC. The accuracy of all indices was
322 computed as the ratio of the number of target areas that had their LCC (or the lack

thereof) correctly detected to the total number of target areas. Additional metrics were also evaluated considering the results grouped in the following categories: a) *detected true*, when the actual LCC year was contained in the 95% confidence interval of the detected LCC year, or when LCC was not detected and an actual LCC process did not occur; b) *time wrong*, when the actual LCC year did not lie in the 95% confidence interval of the detected LCC year; c) *false negative*, when the LCC was not detected, but it has actually occurred, and; d) *false positive*, when LCC was detected, but it has not occurred.

Subset I illustrate the pattern of LCC and the ability of the proposed methodology to identify these sequential clearings (Fig. 3). Within this area, pixels exhibiting LCC in the same year were encompassed within the same patch. The median was calculated for the detected LCC year of all pixels within each patch, providing a quantitative comparison with the actual LCC year. The median rather than the mean was used as a summary measure because it is a robust statistic of central tendency, less influenced by extreme values (outliers). Additionally, the Kendall rank correlation coefficient (τ) between the median of the detected LCC year and the actual vegetation clearing year for the nine patches was also calculated and its statistical significance tested. Subset II was used in a visual analysis between the breakpoints detected by SA time series and Landsat images (false colour composite) at 5-year intervals.

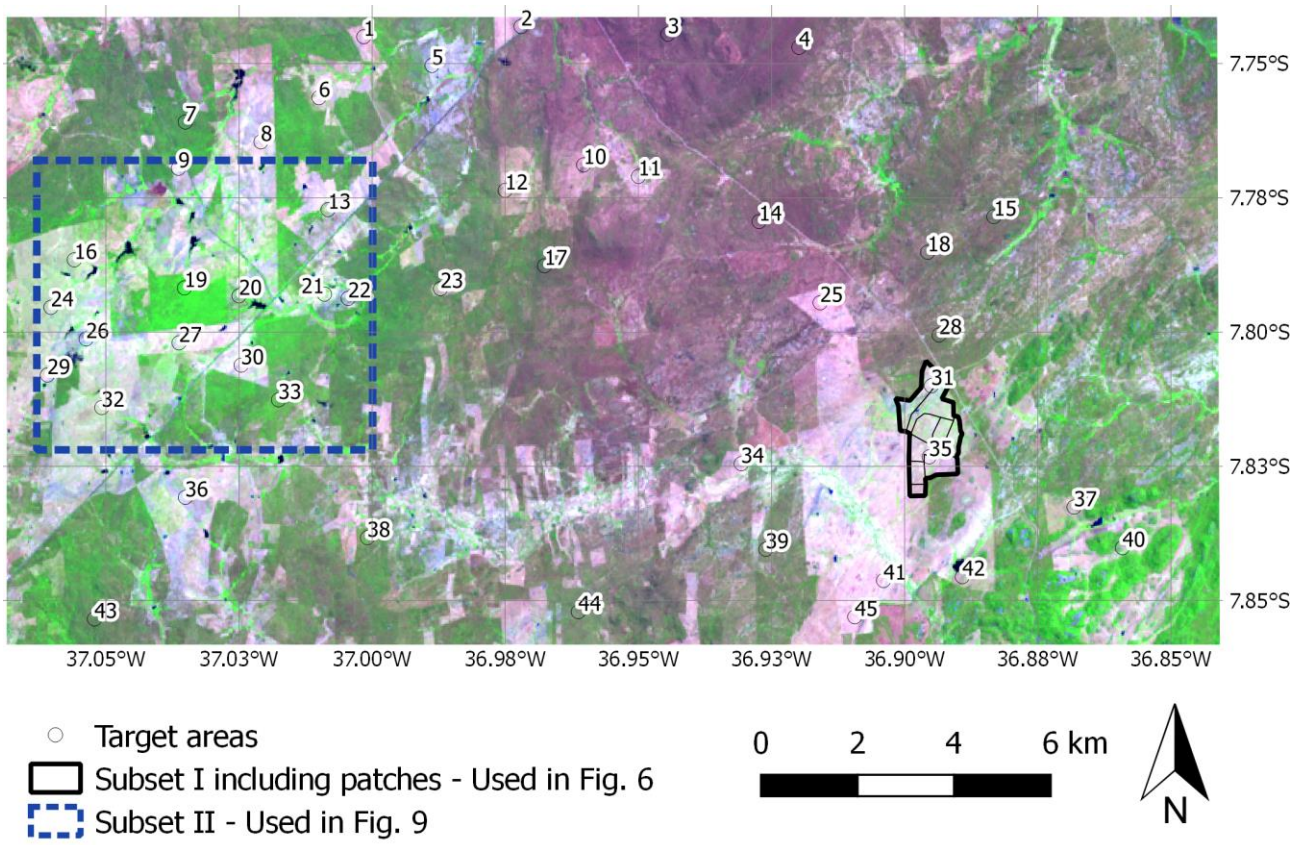

Fig. 3 - Location of the validation sites in the study area: 45 target areas (numbered, 31 target areas where a LCC actually occurred and 14 areas with preserved natural vegetation), the Subset I that had a sequential land-cover clearing process during 2003–2012 and the Subset II validation area. Source: Landsat 8 false colour composite (RGB to bands 5, 4 and 3).

4. Results

Our analyses show that the two main differences between SA, EVI and NDVI are the range of values (Fig. 4), and the average number of breakpoints detected by the structural change component of the TSS-RESTREND method (Table 2). Whereas values ranged between 0.08 and 0.57 for EVI and 0.13 and 0.73 for NDVI, SA values varied only between 0.10 and 0.25. Moreover, the number of the breakpoints detected is greater by using EVI and NDVI than SA (Fig. 4). Most of the breakpoints occurred during a drought period (SPEI < -1, Fig. 2), especially for EVI and NDVI.

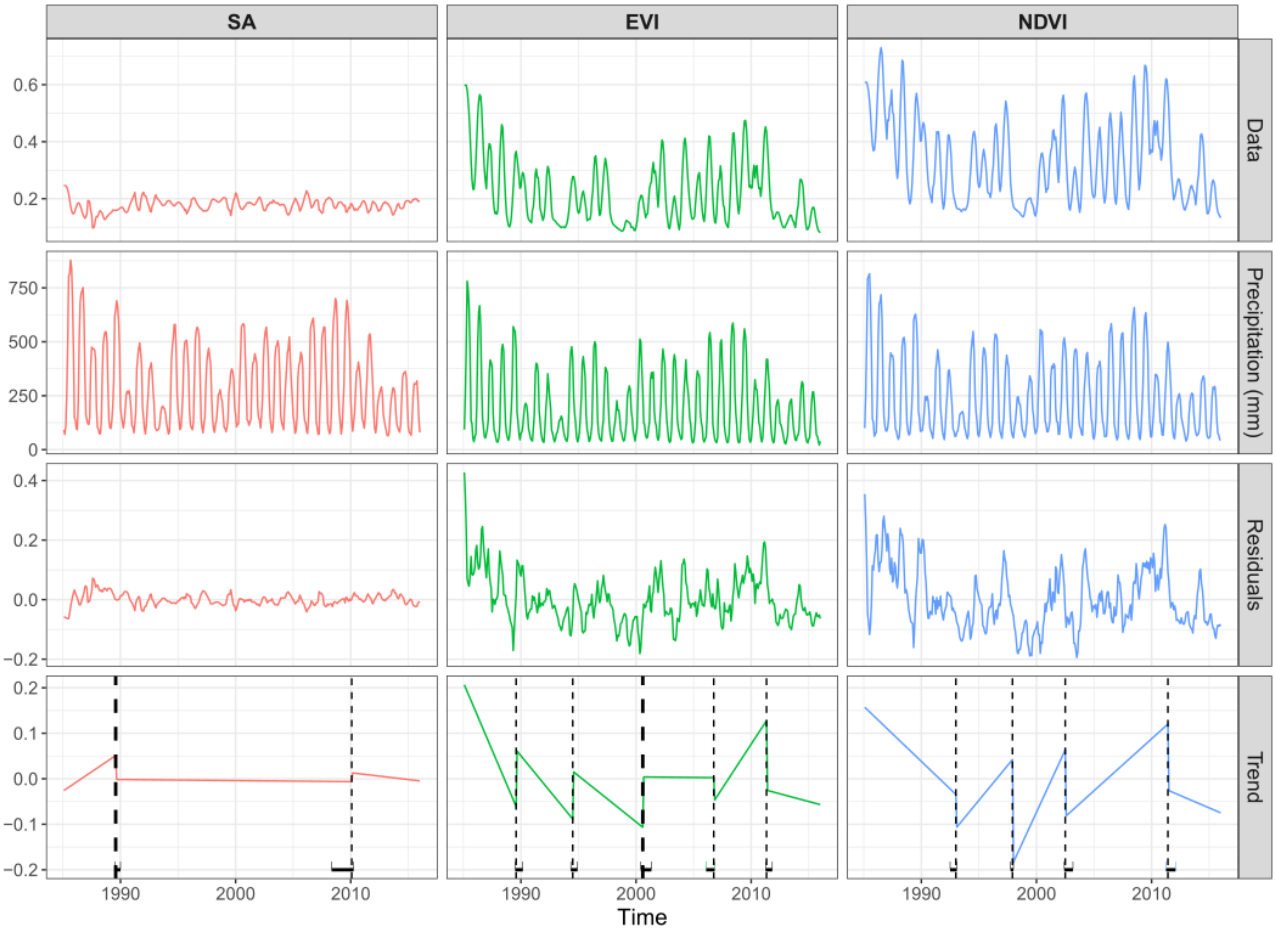

Fig. 4: TSS-RESTREND structural change detection outputs for the target area 22. Top row panel shows SA, EVI and NDVI entire time series data, whereas the next panel has complete OPA time series, followed by monthly residuals of OPA, and Trend to each time series spectral indices. In the Trend panel, vertical lines represent breakpoints and the bold vertical line the most significant breakpoint.

In general, despite the smallest number of breakpoints identified by SA, this index showed the best performance in detecting LCC on an annual scale and had on average the narrowest 95% confidence interval for the breakpoint date when compared to that of EVI and NDVI (Fig. 5, Table 2). The SA detected 89% of the LCC (being the sum of detected true and time wrong), while EVI and NDVI detected only 44% and 46%, respectively (Table 2). The low performance of EVI and NDVI is reflected by the great number of false negatives, representing 36–40%, whereas the false negatives were only 4% for SA. The total false positives represented over 15% for EVI and NDVI, and 7% for SA.

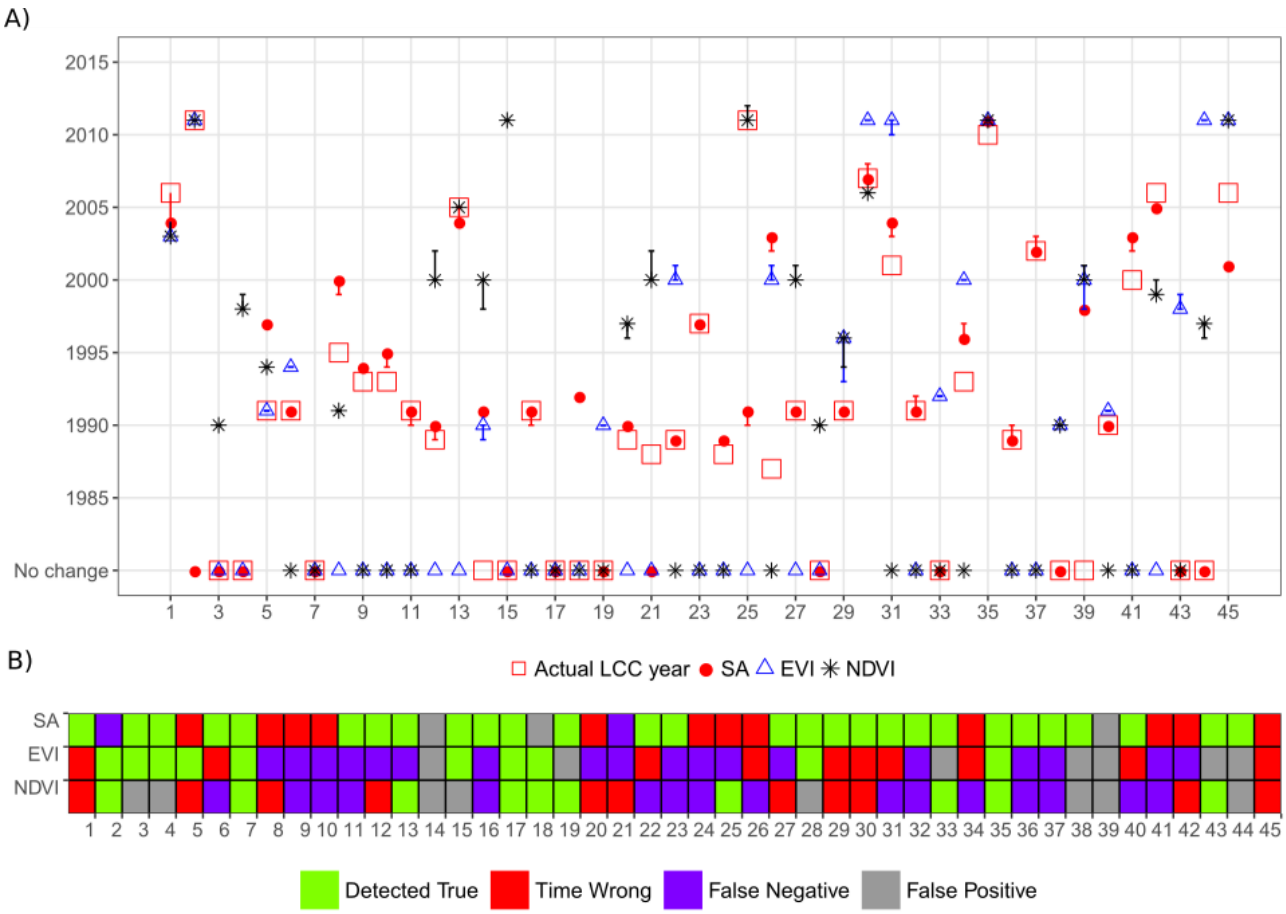

Fig. 5 – Detected and actual year of land-cover clearing for SA, EVI and NDVI for the 45 target areas: A) Description and B) Summary

Subset I (see Fig. 3) was used to analyse the results in more detail. This region contains two of the 45 target areas: in the target area 31 LCC was only detected by SA, while the LCC for target area 35 was correctly detected by all three indices (Fig. 5). Within the subset I, the main changes in land cover occurred between 2003 and 2012, which is shown by nine patches (Fig. 6). Each patch is identified by the actual LCC year that is dominant among its pixels. The analysis of these patches revealed that when EVI and NDVI were used, a substantial number of pixels (sometimes > 40%) were categorized as false negative (Fig. 7A). This situation was particularly relevant in the patches where the LCC occurred in 2003, 2004, 2008 and 2010 (Fig. 6 and 7A). In contrast, results obtained with SA showed that false negative pixels were less than 10% for all patches (Fig. 7A) and exhibited an overall better accuracy in identifying the

actual LCC year (Fig. 7B). In fact, for the nine patches, the median of the detected LCC year by SA was closer to the actual LCC year compared to that by EVI and NDVI (Fig. 7B). This was also confirmed by Kendall's correlation coefficient (τ) between actual and detected LCC years: SA had the highest value (τ = 0.86) with the highest significance ($p < 0.01$).

Table 2 – Number of validation target areas in the different categories (and percentage of the total) according to the results of the TSS-RESTREND method applied with the three spectral indices (Fig. 5), average confidence interval amplitude and average number of breakpoints detected.

Index	Detected true	Time wrong	False positive	False negative	Average 95% confidence interval amplitude (in months)	Average number of breakpoints detected by target area
SA	28 (62%)	12 (27%)	3 (7%)	2 (4%)	8.7	2.8
EVI	10 (22%)	10 (22%)	7 (16%)	18 (40%)	10.9	3.5
NDVI	10 (22%)	11 (24%)	8 (18%)	16 (36%)	11.6	4.0

The best performance of EVI and NDVI was observed for the patches where the clearing of vegetation took place in 2011 and 2012 (Figs. 6 and 7). However, for the other years and for many pixels, the detected LCC year was close to years of a severe drought (1993 and 2000, see Fig. 2). The foremost detected breakpoint years are the drought years of 1990 and 2000, and the period around 2010 (Fig. 8). Although there is a higher variability of the SA results within the patches than those of EVI and NDVI, the median of the detected year of change per patch is closer to the observed date when using the SA (Figs. 7B and 8). Furthermore, while the outlines of the patches are hardly identified in the output raster of the two vegetation indices, they are quite well-defined in the SA raster (Fig. 6).

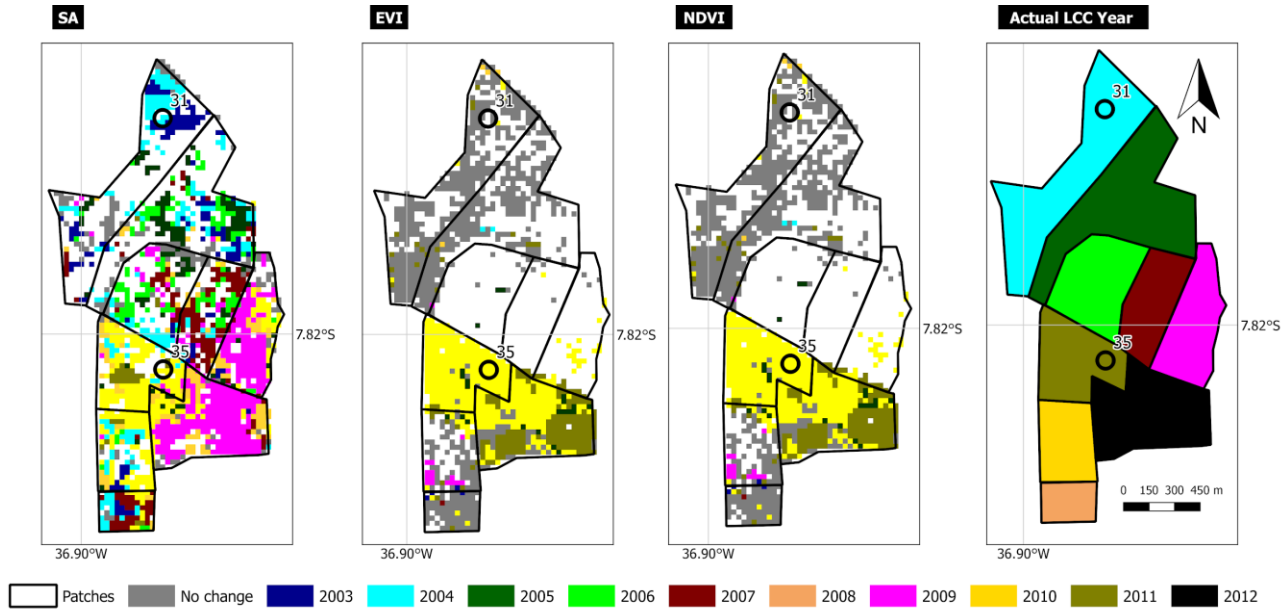

403

404 Fig. 6 – Polygon (subset I) with patches showing the detected breakpoint years of LCC for SA, EVI,

405 NDVI and actual LCC year.

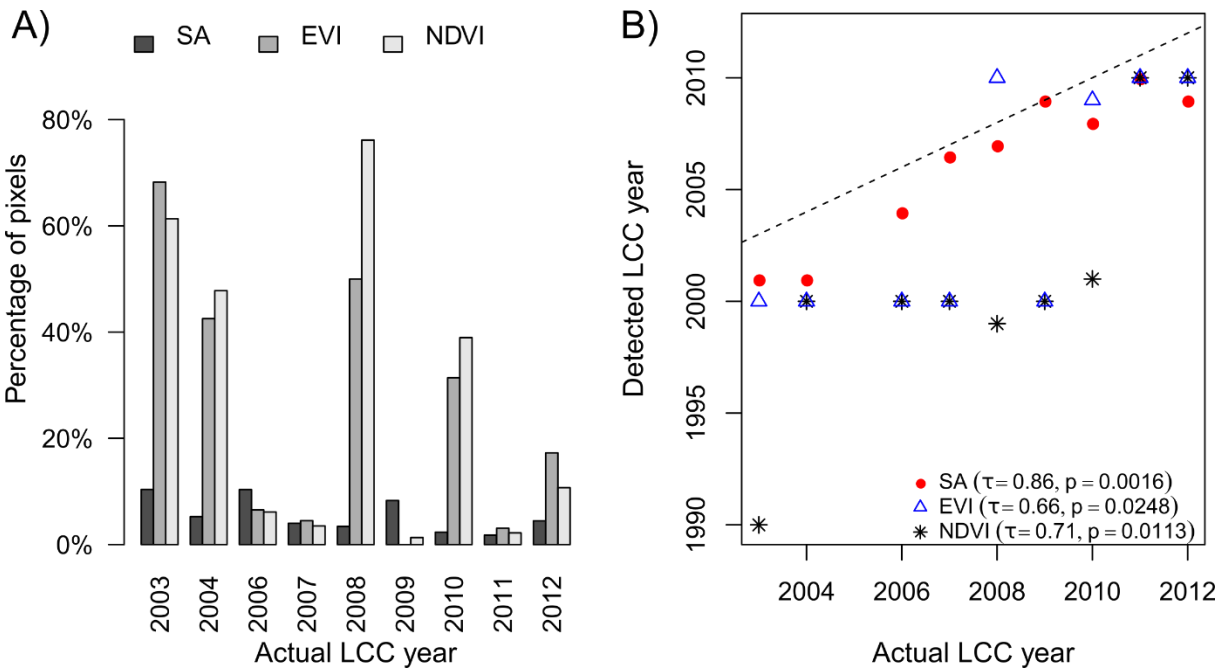

406

407 Fig. 7 - Observed change year LCC for the patches compared with the results of TSS-RESTREND for

408 SA, NDVI and EVI: A) percentage of pixels in each patch classified as false negative; B) median of the

409 detected LCC for all pixels within a patch. The dotted line is the 1:1 line and τ is the Kendall rank

410 correlation coefficient.

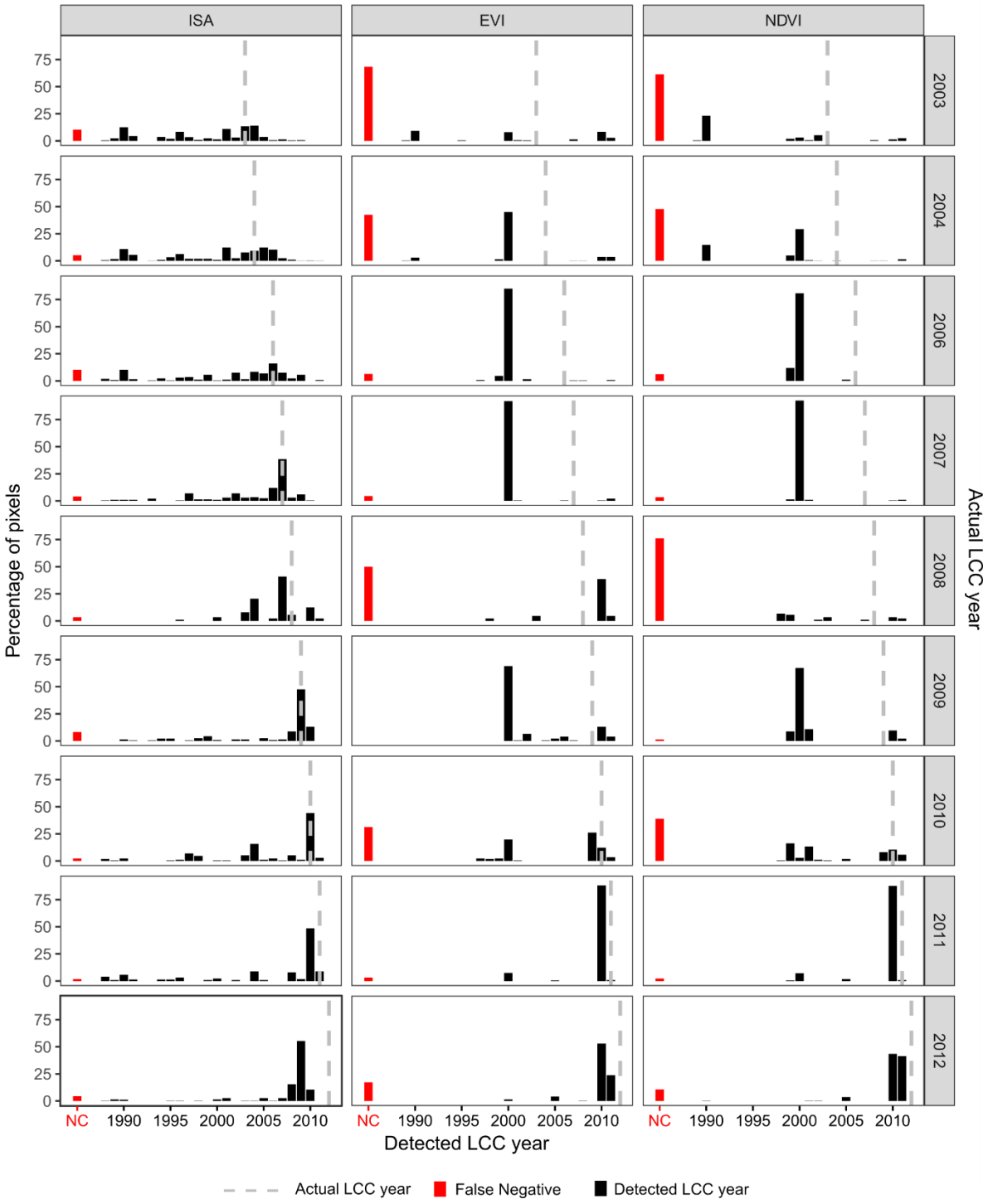

Fig. 8 – Barplots of the detected LCC year obtained by TSS-RESTREND for the three spectral indices (SA, EVI and NDVI) for the patches of the Subset I region. The height of each black bar is the percentage of pixels where a change was detected in that year. Red bars correspond to pixels where no change was detected. Grey dashed lines show observed LCC years.

Visual comparison of the breakpoint raster for subset II region (see Fig. 3) with a Landsat false colour composite shows that SA has some difficulty in identifying the

correct year of clearing when it occurs during the initial and final years of the time series (1985–1988 and 2012–2015, Fig. 9 and supplementary material Fig. S6). On the other hand, SA performed well for small vegetation patches that remained unchanged during the study period (e.g., the region where target area 19 is located).

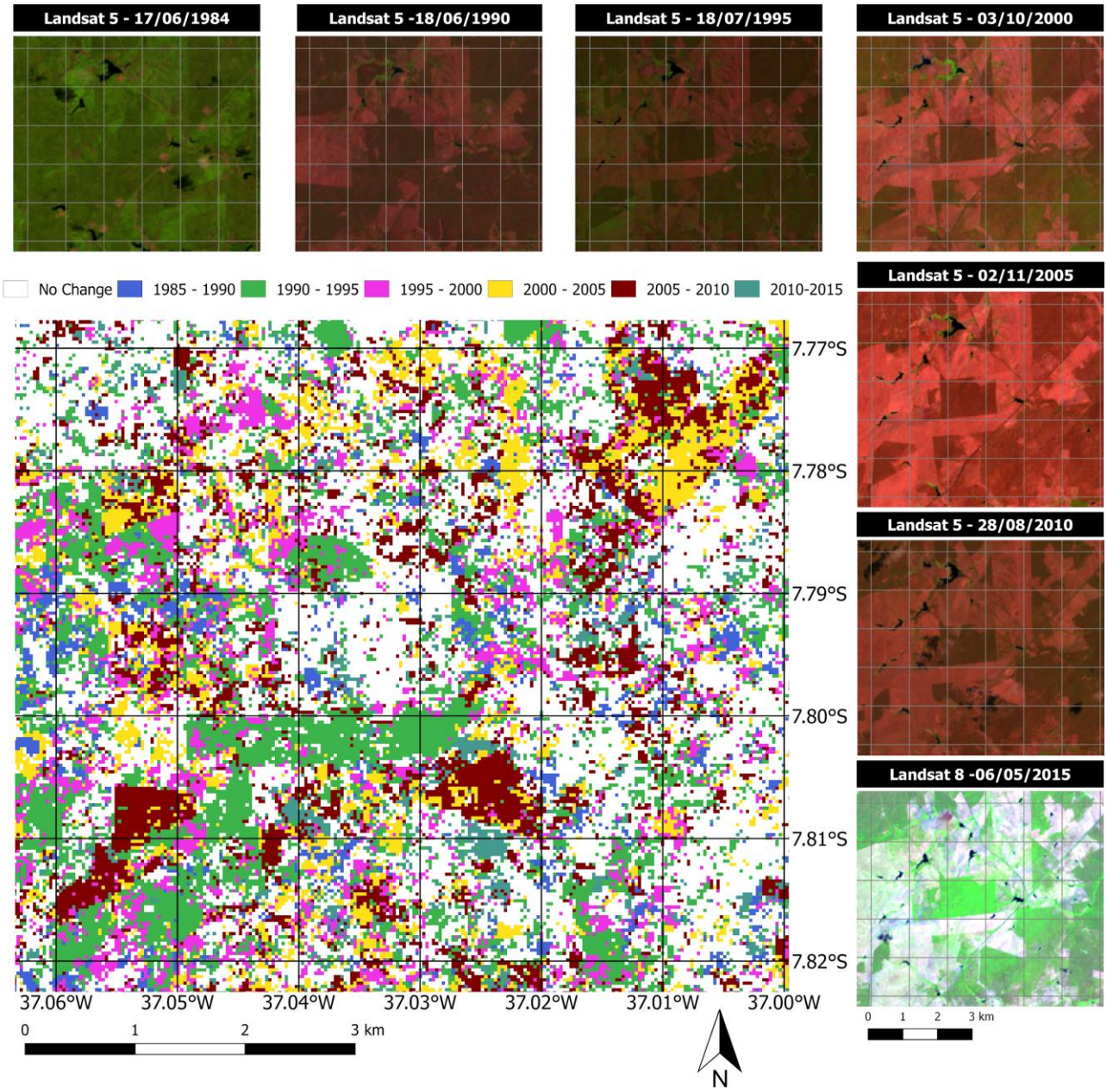

Fig. 9 - Detected LCC year by the TSS-RESTREND based on SA time series for the Subset II highlighted in Fig. 3. Image source: Landsat 5 (RGB to 4, 3 and 2) and Landsat 8 (RGB to 5, 4 and 3) false colour composite.

5. Discussion

Our study suggests that in seasonally dry forests, particularly the Brazilian Caatinga, neither EVI nor NDVI are reliable spectral indices for identifying LCC from Landsat time series. There are difficulties to distinguish deciduous vegetation from the underlying ground during the dry period by indices that use only the VIS–NIR domain (Jacques et al., 2014; Mayes et al., 2015). Despite the wide acceptance of using EVI (Dutrieux et al., 2015) and NDVI (Leroux et al., 2017) to separate the effects of climate variability from anthropogenic impact, and for trend analysis in many different ecosystems (Burrell et al., 2017), these indices exhibited a low performance in detecting the correct timing of LCC in our study. For EVI and NDVI a high number of false negatives (see Table 2, and Figs. 6 and 7A), and the matching between actual and detected LCC years were less than 25%, which is far from an acceptable standard for detecting LCC (Aguirre-Gutiérrez et al., 2012; Mas, 1999).

Climate variability has a strong influence on EVI and NDVI in seasonally dry forests (Guan et al., 2015; Walker et al., 2015) and, therefore, climate effects on land-cover is fundamental to be considered in LCC analysis in these ecosystems. Despite the TSS-RESTREND method providing an approach to remove the effect of precipitation seasonality from the indices, these vegetation indices still show an effect due to extended drought periods. The years with the most severe droughts in the time series were 1990, 1993, 1998, and 2012. When LCC occurred near these years, EVI and NDVI exhibited a circumstantial good efficiency in identifying LCC, which was the case in 1990 and, especially, 2012. While 2011 was a wet year (maximum SPEI > 2.4), 2012 was the beginning of an extremely dry period under drought conditions (SPEI < -0.5) and with rainfall amounts below the total average (see Fig. 2). On the other hand, considering the 14 target areas where no LCC occurred, the accuracy of EVI and NDVI

was 50% and 43%, respectively. In comparison, SA's accuracy was 79% (Fig. 5). We interpret this as an effect of adverse climate period or degradation on the vegetation. Although the NDVI and EVI might show ability to detect intra-annual phenological changes and trends of vegetation degradation (Dutrieux et al., 2015; Leroux et al., 2017), their skill to detect LCC or the lack thereof was quite poor in the present study.

SA exhibited a greater sensitivity to changes involving characteristics other than the greenness of leaves because this index covers other bands (SWIR 1 and SWIR 2) of the electromagnetic spectrum (Lui et al., 2017; Zhao et al., 2018), which are not used by indices that cover only the VIS–NIR. When a soil–plant–atmosphere system is altered by an action of deforestation, the leafless woody biomass — which represents ca. 95% of the aboveground biomass in the Caatinga (Silva and Sampaio, 2008) — is removed and consequently causes the total exposure of the soil to solar radiation. As a consequence of the LCC, the light attenuation, represented by the light extinction coefficient and known to be substantial for deciduous shrublands (Aubin et al., 2000; Domingo et al., 2000), is drastically decreased and thus, the SA increases. This response pattern of SA to LCC manifests regardless of the leaf status in the Caatinga. In comparison to SA, we could not identify any physiological driver or pattern that leads to EVI or NDVI signal alteration when the leafless woody biomass of the Caatinga is removed. The detection of LCC from EVI and NDVI time series seems to be masked considerably by intra-seasonal climate anomalies, especially extended droughts.

Since soil moisture has a high influence on SA, the spectral signals from dry and wet bare soil from any same site can be significantly different (He et al., 2014; Matthias et al., 2000). Therefore, the variation of SA values should be interpreted with caution when addressing LCC analysis. Like in most of the Caatinga region, the soils

of our study area are shallow and present a low water storage capacity (Medeiros et al., 2018). When land cover is cleared, the root zone storage is reduced, and, as a result, SA increases. However, in soils with greater depth and water retention capacities, SA may present lower performance as an indicator of LCC. Spectral indices that use the NIR and the SWIR bands also show a better ability to detect plant phenology than that of NDVI and EVI (Jin et al., 2013) by being more sensitive to the water content of vegetation and soil (Rodríguez-Caballero et al., 2015, Zhao et al., 2018). The SWIR band provides a robust means to estimate the extent of bare soil and vegetation cover in arid and semi-arid regions (Asner and Lobell, 2000). Indices that use the SWIR domain, such as the Soil Tillage Index (STI) and Tasseled Cap Wetness (TCW), exhibited good performance in identifying the variance of dry masses in the Sahel (Jacques et al., 2014) and LCC processes in southern Ethiopia (DeVries et al., 2015). We ascribe to soil moisture the cause of the errors in detecting the actual LCC year when using SA for the target areas 25 and 26. A substantial part of these two areas is covered by ephemeral stream beds. Despite exhibiting no surface water most of the years, the stream beds are known for acting as small aquifers by storing water in the alluvial deposits and increasing the soil moisture along stream channels (Fontes Junior and Montenegro, 2017).

The SA exhibited a high performance in detecting the actual LCC year (62%) and an overall accuracy of detecting LCC (89%) or the lack of it (79%) for all the 45 target areas. For the target areas where the LCC was detected using SA, 39% were detected outside the confidence interval (time wrong) and only 6% were false negatives. We attribute the imprecision in identifying the actual LCC year to some adverse effects of the ecosystem response to LCC on the SA. After vegetation removal, the remaining plant ecosystem, i.e., underground roots and soil, needs some

time to adapt to the new conditions (Saco et al., 2018), which can cause a gradual loss of the root zone storage (D'Odorico et al., 2013), and, consequently, a delay in the full bare soil SA response, which in turn will cause a "time wrong" score for the detected LCC year that is after the actual one. Another aspect to consider is that some LCC activities in the Caatinga occur at very small scales (e.g. activities on one-man farms) and they might overlap two consecutive years until the disturbance is reflected in the SA and qualified as a breakpoint in the time series analysis (Pinheiro et al., 2013). We believe that the target areas 9, 10, 20 and 24 exhibit a 1-year delay for the detection of the actual LCC year. These four areas are located in the upper-left quadrant in Fig. 3, and their LCC occurred between 1988 and 1993, which was a period when this area was densely vegetated and then cleared during a highly fragmented LCC process (see Fig. 9). If this 1-year delay is added to the confidence interval of the detected LCC years, the time wrong rate is reduced from 39 to 26%. This is a decrease of 40% in the time wrong detections, whereas the same 1-year delay tolerance only reduces 20% and 9% of EVI and NDVI time wrong LCC detections, respectively. However, despite the satisfactory accuracy of SA to detect abrupt structural changes (LCC) or their absence, the efficiency of this index to detect long-term degradation trends still needs further research. This is out of the scope of our study, but it is still a very relevant topic to understand land-cover change dynamics. In this respect, vegetation indices, such as EVI and NDVI, have been successfully applied in many different ecosystems around the world for trend analysis (Burrell et al., 2017; Dutrieux et al., 2015).

The TSS-RESTREND method was built upon two previous approaches to analyse changes in land cover, i.e., BFAST and RESTREND, taking advantage of their individual skills. We used the structural change component of the TSS-RESTREND, which has three main characteristics that were fundamental to identify an efficient

indicator of LCC in the Caatinga: the ability to (i) remove the influence of the main climatic variable linked to the phenology in this region (the precipitation), (ii) detect, within the time series, structural significant changes in land cover, and (iii) select the most significant changes. The TSS-RESTREND, a method conceived, developed and validated to be used with vegetation indices, was also efficient when used with SA. The combination of TSS-RESTREND and SA was appropriate to identify LCC in our Caatinga study area. In most cases, in the Caatinga, clearing is followed by subsistence farming or livestock occupation with only few underbrush or grass that sustained the higher SA response, qualifying the clearing as the most significant breakpoint in the time series analysis of the TSS-RESTREND. The slow reestablishment of native vegetation on bare soil areas upon abandonment is due to the low natural fertility condition of the shallow, heterogeneous soils of the Caatinga (Salcedo et al., 1997; Sobrinho et al., 2016) and adverse climate (Althoff et al., 2016).

The two and only false negatives detected by the SA time series (target areas 2 and 21) represent areas that had their vegetation cover removed in either the first or last four years of the time series, i.e., 1985–1988 and 2012–2015 (Fig. 5). In these intervals TSS-RESTREND exhibited limitations in detecting breakpoints. As in other time series analysis methods, errors at the beginning or at the end of any finite-length time series are a common issue (Torrence and Compo, 1998). The concept of the BFAST algorithm (Bai, 1997; Verbesselt et al., 2010), one of the main components of TSS-RESTREND, requires a minimum amount of data values between successive breakpoints and at the beginning and the end of the times series to be able to identify a structural change (Supplementary material Fig. S6). In addition, the conclusions that are drawn from statistical significance tests (e.g., the Chow test) based on a small sample can be unreliable because the null hypothesis that corresponds to a non-

551 significant breakpoint will hardly be rejected at the standard significance levels.
552 Therefore, the use of long time series is essential to reduce this uncertainty. In our
553 study, most of the LCC occurred in the 1990s after the first five years of the time series.
554 The Landsat dataset was a valuable source of information by providing long time series
555 where these LCC processes could be evaluated with a low impact from these edge
556 effects.

557 The limitations in LCC detection for the indices that use only the VIS–NIR
558 domain found here are apparently neither associated with the Landsat temporal
559 resolution nor with the proportion of gap-filling. In fact, looking at the number of months
560 that needed to be gap-filled in the actual year of LCC for each target area it is possible
561 to observe that both EVI and NDVI indices did not show lower error rates when actual
562 LCC years exhibited the lowest gap-filling (less or equal than two months). Besides,
563 there is also no pattern associated with the number of gaps within an actual LCC year
564 and the indices accuracy. EVI and NDVI performed the best when the actual LCC years
565 had approximately 50% of gaps in a year, and they equally exhibited high error rates
566 when the series was minimally (up to 17%) or maximally (up to 67%) gap filled (details
567 can be found in the Supplementary material Table S1 and Figs. S1 to S5). The use of
568 sensors with higher temporal resolution that aggregate rather than gap fill information
569 is an alternative approach that can be used to assess the performance of EVI and
570 NDVI to detect LCC.

571 Our study supports further research towards a better understanding of Caatinga
572 land-cover dynamics. When considering the scale at which these biophysical variations
573 can impact large ecosystems such as the Caatinga, not only the carbon balance is
574 affected, but also the energy and water balances (Bonan, 2008). Although LCC causes
575 a radiative cooling effect due to the increase of SA, this is unbalanced by associated

decreases in evapotranspiration and in surface roughness (Sanderson et al., 2012), which have consequences to regional and global climate, as evidenced by model experiments (Perugini et al., 2017). Based on our work, further analysis and developments in this direction should consider: (i) a deep analysis of SA and other spectral indices applications in LCC studies in other seasonal tropical dry forests; (ii) a cross-related analysis of SA and other variables, such as biomass, evapotranspiration and soil moisture, supported by field-based and remote sensing data; (iii) the suitability of TSS-RESTREND to identify other processes of land-cover alteration, such as degradation and fragmentation, not directly covered in our study, and; (iv) the use of other remote sensing products, such as MODIS and AVHRR, to verify the applicability of SA and vegetation indices in identifying LCC in seasonally dry forests at other spatial scales.

6. Conclusions

We applied the TSS-RESTREND method to a 31-year Landsat time series of SA, EVI and NDVI to evaluate the performance of these indices to detect LCC in the Brazilian Caatinga, a tropical seasonally dry forest. We found that SA outperforms EVI and NDVI in detecting LCC, and that the structural change detection component of TSS-RESTREND is appropriate to identify LCC in space and time.

The spatial resolution and temporal coverage series of Landsat images allows a systematic assessment of altered targets on the land surface, laid out in a complex and fragmented pattern characteristic of the anthropogenic LCC in our study area. The concept of the TSS-RESTREND method is compatible with the reality of the LCC dynamics in this seasonally dry forest, since the selection of the most significant breakpoint unveils the LCC without subsequent vegetation reestablishment.

The lower performance of the EVI and NDVI indices in the detection of LCC in the Caatinga is explained by their high sensitivity to leaf cover variations as a result of seasonal or extreme dry conditions. Changes in land cover affect the entire soil–plant–atmosphere continuum: not only by the removal of biomass and modification of the soil properties, but also in the microclimate, due to direct exposure of the soil to radiation, precipitation and wind. Based on the potential changes that LCC cause in an ecosystem, studies should not rely only on vegetation indices, but should also make use of other spectral ranges that will support a better representation of peculiar ecosystem characteristics.

Acknowledgments

This work has been funded by the Brazilian National Council for Scientific and Technological Development (grant numbers 490115/2013-6 and 310789/2016-8) and the European Commission (grant number FP7-614048) through the EUBrazilCC project (http://eubrazilcloudconnect.eu/), CAPES-ANA (grant number 88887.115880/2015-01), and CAPES/PDSE (grant number 88881.134740/2016-01). This work also forms part of the UK/Brazil Nordeste project funded jointly through the UK Natural Environment Research Council (NE/N012526/1 ICL and NE/N012488/1 UoR) and the Fundação de Amparo à Pesquisa do Estado de São Paulo (2015/50488-5). The Forest Research Centre (CEF) is a research unit funded by Fundação para a Ciência e a Tecnologia I.P. (FCT), Portugal (UID/AGR/00239/2013). We would like to thank the constructive feedback from the editors and three anonymous reviewers.

References

Aguirre-Gutiérrez, J., Seijmonsbergen, A.C., Duivenvoorden, J.F., 2012. Optimizing land cover classification accuracy for change detection, a combined pixel-based and object-based approach in a mountainous area in Mexico. Applied Geography.

628 34, 29–37. doi:10.1016/j.apgeog.2011.10.010

629 Albuquerque, U.P., de Lima Araújo, E., El-Deir, A.C.A., de Lima, A.L.A., Souto, A.,
630 Bezerra, B.M., Ferraz, E.M.N., Maria Xavier Freire, E., Sampaio, E.V. de S.B.,
631 Las-Casas, F.M.G., de Moura, G.J.B., Pereira, G.A., de Melo, J.G., Alves Ramos,
632 M., Rodal, M.J.N., Schiel, N., de Lyra-Neves, R.M., Alves, R.R.N., de Azevedo-
633 Júnior, S.M., Telino Júnior, W.R., Severi, W., 2012. Caatinga Revisited: Ecology
634 and Conservation of an Important Seasonal Dry Forest, The Scientific World
635 Journal. 2012, 1-18. doi:10.1100/2012/205182

636 Althoff, T. D., Menezes, R. S. C., de Carvalho, A. L., de Siqueira Pinto, A., Santiago,
637 G. A. C. F., Ometto, J. P. H. B., Sampaio, E. V., 2016. Climate change impacts
638 on the sustainability of the firewood harvest and vegetation and soil carbon stocks
639 in a tropical dry forest in Santa Teresinha Municipality, Northeast Brazil. Forest
640 Ecology and Management. 360, 367–375. doi:10.1016/j.foreco.2015.10.001

641 Alvares, C.A., Stape, J.L., Sentelhas, P.C., De Moraes Gonçalves, J.L., Sparovek, G.,
642 2013. Köppen's climate classification map for Brazil. Meteorologische Zeitschrift
643 22, 711–728. doi:10.1127/0941-2948/2013/0507

644 Andrade-Lima, D, 1981. The caatinga dominium. Revista brasileira de Botânica, 4,
645 149-163.

646 Andrade-Silva, A.C.R., Nemésio, A., de Oliveira, F.F., Nascimento, F.S., 2012. Spatial-
647 Temporal Variation in Orchid Bee Communities (Hymenoptera: Apidae) in
648 Remnants of Arboreal Caatinga in the Chapada Diamantina Region, State of
649 Bahia, Brazil. Neotropical Entomology. 41, 296–305. doi:10.1007/s13744-012-
650 0053-9

651 Anyamba, A., Small, J.L., Tucker, C.J., Pak, E.W., 2014. Thirty-two Years of Sahelian
652 Zone Growing Season Non-Stationary NDVI3g Patterns. Remote Sensing 6,
653 3101–3122. doi:10.3390/rs6043101

654 Araújo, E.L., Castro, C.C., Albuquerque, U.P., 2007. Dynamics of Brazilian Caatinga –
655 A Review Concerning the Plants, Environment and People. Functional
656 Ecosystems and Communities 1: 15-28

657 Araújo, V.F.P., Bandeira, A G., Vasconcellos, A, 2010. Abundance and stratification of
658 soil macroarthropods in a Caatinga Forest in Northeast Brazil. Brazilian Journal
659 of Biology. 70,737–46.doi:10.1590/S1519-69842010000400006

660 Asner, G. P., Lobell, D. B., 2000. A Biogeophysical Approach for Automated SWIR
661 Unmixing of Soils and Vegetation. Remote Sensing of Environment. 74, 99–112.
662 doi:10.1016/s0034-4257(00)00126-7

663 Aubin, I., Beaudet, M., Messier, C., 2000. Light extinction coefficients specific to the
664 understory vegetation of the southern boreal forest. Canadian Journal of Forest
665 Research. 30,168–177. doi: 10.1139/x99-185

666 Bai, J., 1997. Estimation of a Change Point in Multiple Regression Models. Review of
667 Economics and Statistics. 79, 551–563. doi:10.1162/003465397557132

668 Beguería, S., Latorre, B., Reig, F., Vicente-Serrano, S.M. 2017. Global SPEI database.
669 http://spei.csic.es/database.html. Access in 11 January 2017.

670 Belchior, M., Tai, D.W., Held, F.C. Von, 2017. Indicadores Instituto Brasileiro de
671 Geografia e Estatística (IBGE). https://www.ibge.gov.br/estatisticas-
672 novoportal/economicas/agricultura-e-pecuaria/9201-levantamento-sistematico-

673 da-producao-agricola.html?&t=destaques. (accessed 03 January 2018)

674 Bonan, G. B., 2008. Forests and climate change: Forcings, feed- backs, and the
675 climate benefits of forests. Science. 320, 1444–1449,
676 doi:10.1126/science.1155121.

677 Brito, A.F., Presley, S.J., Santos, G.M.M., 2012. Temporal and trophic niche overlap
678 in a guild of flower-visiting ants in a seasonal semi-arid tropical environment,
679 Journal of Arid Environments. 87, 161-167. doi:10.1016/j.jaridenv.2012.07.001

680 Burrell, A.L., Evans, J.P., Liu, Y., 2017. Detecting dryland degradation using Time
681 Series Segmentation and Residual Trend analysis (TSS-RESTREND). Remote
682 Sensing of Environment. 197, 43-57. doi:10.1016/j.rse.2017.05.018

683 Burrell, A.L., Evans, J.P., Liu, Y., 2018. The impact of dataset selection on land
684 degradation assessment. ISPRS Journal of Photogrammetry and Remote
685 Sensing. 146, 22-37. doi: 10.1016/j.isprsjprs.2018.08.017

686 Cadier, E. 1996. Small watershed hydrology in semi-arid north-eastern Brazil: basin
687 typology and transposition of annual runoff data. Journal of Hydrology.182, 117–
688 141. doi: 10.1016/0022-1694(95)02933-8

689 Cao, R., Chen, Y., Shen, M., Chen, J., Zhou, J., Wang, C., Yang, W, 2018. A simple
690 method to improve the quality of NDVI time-series data by integrating
691 spatiotemporal information with the Savitzky-Golay filter. Remote Sensing of
692 Environment. 217, 244–257. doi:10.1016/j.rse.2018.08.022

693 Chen, J., Jönsson, P., Tamura, M., Gu, Z., Matsushita, B., Eklundh, L., 2004. A simple
694 method for reconstructing a high-quality NDVI time-series data set based on the
695 Savitzky-Golay filter. Remote Sensing of Environment. 91, 332–344.
696 doi:10.1016/j.rse.2004.03.014

697 Chow, G.C., 1960. Tests of equality between sets of coefficients in two linear
698 regressions. Econometrica. 28,591–605. doi:10.2307/1910133.

699 CNUC, 2018 - Cadastro Nacional de Unidades de Conservação (Brazilian National
700 Database of Conservation Units). http://www.mma.gov.br/areas-
701 protegidas/cadastro-nacional-de-ucs (accessed in 02 Oct-2018)

702 Daughtry, C.S.T., 2001. Discriminating Crop Residues from Soil by Shortwave Infrared
703 Reflectance. Agronomy Journal. 93, 125-131. doi:10.2134/agronj2001.931125x

704 De Jong, R., Verbesselt, J., Schaepman, M.E., de Bruin, S., 2012. Trend changes in
705 global greening and browning: Contribution of short-term trends to longer-term
706 change. Global Change. Biology. 18, 642-655. doi:10.1111/j.1365-
707 2486.2011.02578.x

708 DeVries, B., Verbesselt, J., Kooistra, L., Herold, M., 2015. Robust monitoring of small-
709 scale forest disturbances in a tropical montane forest using Landsat time series.
710 Remote Sensing of Environment. 161, 107-121. doi:10.1016/j.rse.2015.02.012

711 D'Odorico, P., Bhattachan, A., Davis, K.F., Ravi, S., Runyan, C.W., 2013. Global
712 desertification: Drivers and feedbacks. Advances in Water Resources. 51, 326–
713 344. doi:10.1016/j.advwatres.2012.01.013

714 Domingo, F., Villagarcia, L., Brenner, A. J., Puigdefabregas, J. 2000. Measuring and
715 modelling the radiation balance of a heterogeneous shrubland. Plant, Cell and
716 Environment. 23, 27–38. doi:10.1046/j.1365-3040.2000.00532.x

717 Dutrieux, L.P., Verbesselt, J., Kooistra, L., Herold, M., 2015. Monitoring forest cover
718 loss using multiple data streams, a case study of a tropical dry forest in Bolivia.
719 ISPRS Journal of Photogrammetry and Remote Sensing.
720 doi:10.1016/j.isprsjprs.2015.03.015

721 Dwyer, J., Roy, D., Sauer, B., Jenkerson, C., Zhang, H., Lymburner, L., 2018. Analysis
722 Ready Data: Enabling Analysis of the Landsat Archive. 10, 1363-1382. doi:
723 10.3390/rs10091363

724 Eckert, S., Hüsler, F., Liniger, H., Hodel, E., 2015. Trend analysis of MODIS NDVI time
725 series for detecting land degradation and regeneration in Mongolia. Journal of
726 Arid Environments. 113, 16–28. doi:10.1016/j.jaridenv.2014.09.001

727 Egorov, A. V., Roy, D.P., Zhang, H.K., Hansen, M.C., Kommareddy, A., 2018.
728 Demonstration of percent tree cover mapping using Landsat Analysis Ready Data
729 (ARD) and sensitivity with respect to Landsat ARD processing level. Remote
730 Sensing. 10, 209-223. doi:10.3390/rs10020209

731 Erasmi, S., Schucknecht, A., Barbosa, M.P., Matschullat, J., 2014. Vegetation
732 greenness in northeastern brazil and its relation to ENSO warm events. Remote
733 Sensing. 6, 3041–3058. doi:10.3390/rs6043041

734 Evans, J., Geerken, R., 2004. Discrimination between climate and human-induced
735 dryland degradation. Journal of Arid Environments. 57, 535–554.
736 doi:10.1016/S0140-1963(03)00121-6

737 Fensholt, R., Langanke, T., Rasmussen, K., Reenberg, A., Prince, S.D., Tucker, C.,
738 Scholes, R.J., Le, Q.B., Bondeau, A., Eastman, R., Epstein, H., Gaughan, A.E.,
739 Hellden, U., Mbow, C., Olsson, L., Paruelo, J., Schweitzer, C., Seaquist, J.,
740 Wessels, K., 2012. Greenness in semi-arid areas across the globe 1981-2007 -
741 an Earth Observing Satellite based analysis of trends and drivers. Remote
742 Sensing of Environment. 121, 144–158. doi:10.1016/j.rse.2012.01.017

743 Flood, N., 2013. Seasonal composite Landsat TM/ETM+ Images using the medoid (a
744 multi-dimensional median). Remote Sensing. 5, 6481–6500.
745 doi:10.3390/rs5126481

746 Fontes Júnior, R.V. de P., Montenegro, A.A. de A., 2017. Temporal dependence of
747 potentiometric levels and groundwater salinity in alluvial aquifer upon rainfall and
748 evapotranspiration. Brazilian Journal of Water Resources 22, 54-63.
749 doi:10.1590/2318-0331.0217170059

750 Funk, C., Peterson, P., Landsfeld, M., Pedreros, D., Verdin, J., Shukla, S., Husak, G.,
751 Rowland, J., Harrison, L., Hoell, A., Michaelsen, J., 2015. The climate hazards
752 infrared precipitation with stations—a new environmental record for monitoring
753 extremes. Scientific Data 2, 150066. doi:10.1038/sdata.2015.66

754 Gómez, C., White, J.C., Wulder, M.A., 2016. Optical remotely sensed time series data
755 for land cover classification: A review. ISPRS Journal of Photogrammetry and
756 Remote Sensing. 116, 55-72. doi:10.1016/j.isprsjprs.2016.03.008

757 Google, 2018. Google Earth Pro. https://www.google.com/earth/ (accessed 03
758 January 2018)

759 Guan, K., Pan, M., Li, H., Wolf, A., Wu, J., Medvigy, D., Caylor, K.K., Sheffield, J.,
760 Wood, E.F., Malhi, Y., Liang, M., Kimball, J.S., Saleska, S.R., Berry, J., Joiner,
761 J., Lyapustin, A.I., 2015. Photosynthetic seasonality of global tropical forests

762 constrained by hydroclimate. Nature Geoscience. 8, 284–289.
763 doi:10.1038/ngeo2382

764 He, C., Tian, J., Gao, B., Zhao, Y., 2015. Differentiating climate and human-induced
765 drivers of grassland degradation in the Liao River Basin, China. Environmental
766 Monitoring and Assessment. 187, 4199. doi:10.1007/s10661-014-4199-2

767 Hein, L., De Ridder, N., Hiernaux, P., Leemans, R., De Wit, A., Schaepman, M., 2011.
768 Desertification in the Sahel: Towards better accounting for ecosystem dynamics
769 in the interpretation of remote sensing images. Journal of Arid Environments. 75,
770 1164–1172. doi:10.1016/j.jaridenv.2011.05.002

771 Helsel, D.R., Hirsch, R.M., 2002. Trend Analysis. Statistical Methods in Water
772 Resources. Techniques of Water-Resources Investigations of the United States
773 Geological Survey. Book 4, Hydrologic Analysis and Interpretation, chapter A3
774 323–355.

775 Higginbottom, T.P., Symeonakis, E., 2014. Assessing land degradation and
776 desertification using vegetation index data: Current frameworks and future
777 directions. Remote Sensing. 6, 9552–9575. doi:10.3390/rs6109552

778 Huete, A., Didan, K., Miura, T., Rodriguez, E.P., Gao, X., Ferreira, L.G., 2002.
779 Overview of the radiometric and biophysical performance of the MODIS
780 vegetation indices. Remote Sensing of Environment. 83, 195–213.
781 doi:10.1016/S0034-4257(02)00096-2

782 Huete, A.R., Liu, H.Q., Batchily, K., J., L. van W., 1997. A comparison of vegetation
783 indices over a global set of TM images for EOS-MODIS. Remote Sensing of
784 Environment, 59, 440–451. doi:10.1016/s0034-4257(96)00112-5.

785 Ibrahim, Y.Z., Balzter, H., Kaduk, J., Tucker, C.J., 2015. Land degradation assessment
786 using residual trend analysis of GIMMS NDVI3g, soil moisture and rainfall in Sub-
787 Saharan West Africa from 1982 to 2012. Remote Sensing. 7, 5471–5494.
788 doi:10.3390/rs70505471

789 INMET, National Institute of Meteorology of Brazil, 2018.
790 http://www.inmet.gov.br/portal/index.php?r=bdmep/bdmep (Accessed January
791 2018)

792 IPCC, 2000. Land Use, Land-Use Change and Forestry. Intergovernmental Panel on
793 Climate Change
794 http://www.ipcc.ch/ipccreports/sres/land_use/index.php?idp=157. (accessed 10
795 October 2018)

796 Jacques, D.C., Kergoat, L., Hiernaux, P., Mougin, E., Defourny, P., 2014. Monitoring
797 dry vegetation masses in semi-arid areas with MODIS SWIR bands. Remote
798 Sensing of Environment. 153, 40–49. doi:10.1016/j.rse.2014.07.027

799 Jin, C., Xiao, X., Merbold, L., Arneth, A., Veenendaal, E., Kutsch, W.L., 2013.
800 Phenology and gross primary production of two dominant savanna woodland
801 ecosystems in Southern Africa. Remote Sensing of Environment. 135, 189–201.
802 doi:10.1016/j.rse.2013.03.033

803 Ju, J., Masek, J.G., 2016. The vegetation greenness trend in Canada and US Alaska
804 from 1984-2012 Landsat data. Remote Sensing of Environment. 176, 1-16
805 doi:10.1016/j.rse.2016.01.001

806 Karlson, M., Ostwald, M., 2016. Remote sensing of vegetation in the Sudano-Sahelian

807 zone: A literature review from 1975 to 2014. Journal of Arid Environments.
808 doi:10.1016/j.jaridenv.2015.08.022

809 Karnieli, A., Qin, Z., Wu, B., Panov, N., Yan, F., 2014. Spatio-temporal dynamics of
810 land-use and land-cover in the Mu Us Sandy Land, China, using the change
811 vector analysis technique. Remote Sensing. 6, 9316–9339.
812 doi:10.3390/rs6109316

813 Katsanos, D., Retalis, A., Michaelides, S., 2016. Validation of a high-resolution
814 precipitation database (CHIRPS) over Cyprus for a 30-year period. Atmospheric
815 Research. 169, 459–464. doi:10.1016/j.atmosres.2015.05.015

816 Lambin, E.F., Geist, H.J., Lepers, E., 2003. Dynamics of land use and land cover
817 change in tropical regions. Annual Review of Environment and Resources. 28,
818 205–241. doi:10.1146/annurev.energy.28.050302.105459

819 Lamchin, M., Lee, J.Y., Lee, W.K., Lee, E.J., Kim, M., Lim, C.H., Choi, H.A., Kim, S.R.,
820 2016. Assessment of land cover change and desertification using remote sensing
821 technology in a local region of Mongolia. Advances in Space Research. 57, 64–
822 77. doi:10.1016/j.asr.2015.10.006

823 Le Toan, T., Quegan, S., Davidson, M.W.J., Balzter, H., Paillou, P., Papathanassiou,
824 K., Plummer, S., Rocca, F., Saatchi, S., Shugart, H., Ulander, L., 2011. The
825 BIOMASS mission: Mapping global forest biomass to better understand the
826 terrestrial carbon cycle. Remote Sensing of Environment. 115, 2850–2860.
827 doi:10.1016/j.rse.2011.03.020

828 Leal, I.R., Da Silva, J.M.C., Tabarelli, M., Lacher, T.E., 2005. Changing the Course of
829 Biodiversity Conservation in the Caatinga of Northeastern Brazil. Conservation
830 Biology. 19, 701–706. doi:10.1111/j.1523-1739.2005.00703.x

831 Leroux, L., Bégué, A., Lo Seen, D., Jolivot, A., Kayitakire, F., 2017. Driving forces of
832 recent vegetation changes in the Sahel: Lessons learned from regional and local
833 level analyses. Remote Sensing of Environment. 191, 38–54.
834 doi:10.1016/j.rse.2017.01.014

835 Li, X.B., Li, R.H., Li, G.Q., Wang, H., Li, Z.F., Li, X., Hou, X.Y., 2016. Human-induced
836 vegetation degradation and response of soil nitrogen storage in typical steppes in
837 Inner Mongolia, China. Journal of Arid Environments. 124, 80-90.
838 doi:10.1016/j.jaridenv.2015.07.013

839 Lima, A.L.A., Rodal, M.J.N., 2010. Phenology and wood density of plants growing in
840 the semi-arid region of northeastern Brazil, Journal of Arid Environments. 74,
841 1363-1373. doi:10.1016/j.jaridenv.2010.05.009

842 Lima, G.D.S., Lima, J.R. de F., Silva, N. da, Oliveira, R.S. de, Lucena, R.F.P., 2016.
843 Inventory in situ of plant resources used as fuel in the Semiarid Region of
844 Northeast Brazil. Brazilian Journal of Biological Sciencies. 3, 45.
845 doi:10.21472/bjbs.030505

846 Linares-Palomino, R., Oliveira-Filho, A.T., Pennington, R.T., 2011. Seasonally Dry
847 Tropical Forests 3–21. doi:10.5822/978-1-61091-021-7

848 Liu, F., Chen, Y., Lu, H., Shao, H., 2017. Albedo indicating land degradation around
849 the Badain Jaran Desert for better land resources utilization. Science of The Total
850 Environment. 578, 67–73. doi:10.1016/j.scitotenv.2016.06.171

851 Liu, J., Shao, Q., Yan, X., Fan, J., Zhan, J., Deng, X., Huang, L, 2016. The climatic

852 impacts of land use and land cover change compared among countries. Journal
853 of Geographical Sciences, 26(7), 889–903. doi: 10.1007/s11442-016-1305-0

854 Loveland, T.R., Dwyer, J.L., 2012. Landsat: Building a strong future. Remote Sensing
855 of Environment. 122, 22–29. doi:10.1016/j.rse.2011.09.022

856 Marengo, J.A., Torres, R.R., Alves, L.M., 2017. Drought in Northeast Brazil—past,
857 present, and future. Theoretical and Applied Climatology. 129, 1189–1200.
858 doi:10.1007/s00704-016-1840-8

859 Mariano, D.A., Santos, C.A.C. dos., Wardlow, B.D., Anderson, M.C., Schiltmeyer, A.
860 V., Tadesse, T., Svoboda, M.D., 2018. Use of remote sensing indicators to assess
861 effects of drought and human-induced land degradation on ecosystem health in
862 Northeastern Brazil. Remote Sensing of Environment. 213, 129–143.
863 doi:10.1016/j.rse.2018.04.048

864 Mas, J. F., 1999. Monitoring land-cover changes : A comparison of change detection
865 techniques. International Journal of Remote Sensing. 20, 139–152.
866 doi:10.1080/014311699213659

867 Masek, J.G., Vermote, E.F., Saleous, N.E., Wolfe, R., Hall, F.G., Huemmrich, K.F.,
868 Gao, F., Kutler, J., Lim, T., 2006. A Landsat Surface Reflectance Dataset for
869 North America, 1990–2000. IEEE Geoscience and Remote Sensing Letters. 3,
870 68–72. doi:10.1109/lgrs.2005.857030

871 Matthias, A.D.D., Fimbres, A., Sano, E.E.E., Post, D.F.F., Accioly, L., Batchily, A.K.K.,
872 Ferreira, L.G.G., 2000. Surface roughness effects on soil albedo. Soil Science
873 Society of America Journal. 64, 1035–1041. doi:10.2136/sssaj2000.6431035x

874 Mayes, M.T., Mustard, J.F., Melillo, J.M., 2015. Forest cover change in Miombo
875 Woodlands: Modeling land cover of African dry tropical forests with linear spectral
876 mixture analysis. Remote Sensing of Environment. 165, 203–215.
877 doi:10.1016/j.rse.2015.05.006

878 Medeiros, I.C., da Costa Silva, J.F.C.B., Silva, R.M., Santos, C.A.G., 2018. Run-off–
879 erosion modelling and water balance in the Epitácio Pessoa Dam river basin,
880 Paraíba State in Brazil. International Journal of Environmental Science and
881 Technology. doi:10.1007/s13762-018-1940-3

882 MMA, Brazilian Ministry of the Environment, 2018. http://geocatalogo.mma.gov.br/
883 (accessed January 2018)

884 Moro, M.F., Lughadha, E.N., Araújo, F.S. de, Martins, F.R., 2016. A Phytogeographical
885 Metaanalysis of the Semiarid Caatinga Domain in Brazil. The Botanical Review.
886 82, 91–148. doi:10.1007/s12229-016-9164-z

887 Munyati, C., Mboweni, G., 2013. Variation in NDVI values with change in spatial
888 resolution for semi-arid savanna vegetation: A case study in northwestern South
889 Africa. International Journal of Remote Sensing. 34, 2253–2267.
890 doi:10.1080/01431161.2012.743692

891 Nagler, P.L., Daughtry, C.S.T., Goward, S.N., 2000. Plant litter and soil reflectance.
892 Remote Sensing of Environment. 71, 207–215. doi:10.1016/S0034-
893 4257(99)00082-6

894 Nouvelot, J. F. 1974. Planificação da implantação de bacias representativas. Recife,
895 SUDENE-DRN.

Padilha, A. L., Vitorello, Í., Pádua, M. B., Fuck, R. A, 2016. Deep magnetotelluric signatures of the early Neoproterozoic Cariris Velhos tectonic event within the Transversal sub-province of the Borborema Province, NE Brazil. Precambrian Research, 275, 70-83.

Paredes-Trejo, F.J., Barbosa, H.A., Lakshmi Kumar, T. V., 2017. Validating CHIRPS-based satellite precipitation estimates in Northeast Brazil. Journal of Arid Environment. 139, 26–40. doi:10.1016/j.jaridenv.2016.12.009

Pereira, I.M., Andrade, L.A., Sampaio, E.V.S.B., Barbosa, M.R. V., 2003. Use-history Effects on Structure and Flora of Caatinga. Biotropica 35, 154–165. doi:10.1111/j.1744-7429.2003.tb00275.x

Perez-Marin, A. Cavalcante, A.M.B., Medeiros, S. Tinôco, L., Salcedo, I.H. 2012. Núcleos de desertificação no semiárido brasileiro: Ocorrência natural ou antrópica?. Parcerias Estratégicas. 17, 87-106.

Perugini, L., Caporaso, L., Marconi, S., Cescatti, A., Quesada, B., de Noblet-Ducoudré, N., Arneth, A. 2017. Biophysical effects on temperature and precipitation due to land cover change. Environmental Research Letters, 12(5), 053002. doi: 10.1088/1748-9326/aa6b3f

Pinheiro, E.A.R., Costa, C.A.G., De Araújo, J.C., 2013. Effective root depth of the Caatinga biome. Journal of Arid Environment. 89, 1–4. doi:10.1016/j.jaridenv.2012.10.003

R Core Team, 2017. R: A language and environment for statistical computing. R Foundation for Statistical Computing, Vienna, Austria. URL https://www.R-project.org/. (Accessed October 2017)

Rodal, M., Barbosa, M., Thomas, W., 2008. Do the seasonal forests in northeastern Brazil represent a single floristic unit? Brazilian Journal of Biology. 68, 467–475. doi:10.1590/S1519-69842008000300003

Rodríguez-Caballero, E., Knerr, T., Weber, B., 2015. Importance of biocrusts in dryland monitoring using spectral indices. Remote Sensing of Environment. 170, 32–39. doi:10.1016/j.rse.2015.08.034

Saco, P.M., Moreno-de las Heras, M., Keesstra, S., Baartman, J., Yetemen, O., Rodríguez, J.F., 2018. Vegetation and soil degradation in drylands: Non linear feedbacks and early warning signals. Current Opinion in Environmental Science & Health. 5, 67–72. doi:10.1016/j.coesh.2018.06.001

Salcedo, I.H., Tiessen, H., Sampaio, E.V.S.B., 1997. Nutrient availability in, soil samples from shifting cultivation sites in the semi-arid Caatinga of NE Brazil. Agriculture, Ecosystems & Environment. 65, 177–186. doi:10.1016/S0167-8809(97)00073-X

Samain, O., Kergoat, L., Hiernaux, P., Guichard, F., Mougin, E., Timouk, F., Lavenu, F., 2008. Analysis of the in situ and MODIS albedo variability at multiple timescales in the Sahel. Journal of Geophysical Research. 113, 1–16. doi:10.1029/2007JD009174

Sanderson M., Pope E., Santini M., Mercogliano P., Montesarchio, M., 2012 Influences of EU forests on weather patterns: Final Report. Report for the European Commission (DG-Environment). http://ec.europa.eu/environment/forests/pdf/EU_Forests_Final_Report.pdf

941 Santos, A. M., Tabarelli, M., 2002. Distance from roads and cities as a predictor of
942 habitat loss and fragmentation in the caatinga vegetation of Brazil. Brazilian
943 Journal of Biology. 62, 897–905. doi:10.1590/S1519-69842002000500020

944 Savitzky, A., Golay, M.J.E., 1964. Smoothing and differentiation of data by simplified
945 least squares procedures. Analytical Chemistry. 36, 1627–1639.
946 doi:10.1021/ac60214a047

947 Schertz, T., Alexander, R., Ohe, D., 1991. The computer program Estimate Trend
948 (ESTREND), a system for the Detection of Trends in Water-quality data U.S.
949 Geological Survey Water Resources Investigations Report 91-4040, 72 p.
950 Reston, VA, USA.

951 Schucknecht, A., Erasmi, S., Niemeyer, I., Matschullat, J., 2013. Assessing vegetation
952 variability and trends in north-eastern Brazil using AVHRR and MODIS NDVI time
953 series. European Journal of Remote Sensing. 46, 40–59.
954 doi:10.5721/EuJRS20134603

955 Schwinning, S., Sala, O.E., Loik, M.E., 2004. Thresholds, memory, and seasonality:
956 understanding pulse dynamics in arid/semi-arid ecosystems. Oecologia 141, 191-
957 193. doi: 10.1007/s00442-004-1683-3

958 Shuai, Y., Masek, J.G., Gao, F., Schaaf, C.B., He, T., 2014. An approach for the long-
959 term 30-m land surface snow-free albedo retrieval from historic Landsat surface
960 reflectance and MODIS-based a priori anisotropy knowledge. Remote Sensing of
961 Environment 152, 467–479. doi:10.1016/j.rse.2014.07.009

962 Silva, G.C., Sampaio, E.V.S.B., 2008. Biomassas de partes aéreas em plantas da
963 caatinga. Revista Árvore. 32, 567-575. ISSN 0100-6762. doi:10.1590/S0100-
964 67622008000300017.

965 Sobrinho, M. S., Tabarelli, M., Machado, I. C., Sfair, J. C., Bruna, E. M. and Lopes, A.
966 V. 2016. Land use, fallow period and the recovery of a Caatinga forest. Biotropica.
967 48,586-597. doi:10.1111/btp.12334

968 Song, X.P., Huang, C., Sexton, J.O., Channan, S., Townshend, J.R., 2014. Annual
969 detection of forest cover loss using time series satellite measurements of percent
970 tree cover. Remote Sensing. 6, 8878–8903. doi:10.3390/rs6098878

971 Steyaert, L. T., Knox, R. G, 2008. Reconstructed historical land cover and biophysical
972 parameters for studies of land-atmosphere interactions within the eastern United
973 States. Journal of Geophysical Research, 113(D2), D02101. doi:
974 10.1029/2006JD008277

975 Stroppiana, D., Bordogna, G., Carrara, P., Boschetti, M., Boschetti, L., Brivio, P.A.,
976 2012. A method for extracting burned areas from Landsat TM/ETM+ images by
977 soft aggregation of multiple Spectral Indices and a region growing algorithm.
978 ISPRS Journal of Photogrammetry and Remote Sensing. 69, 88–102.
979 doi:10.1016/j.isprsjprs.2012.03.001

980 Torrence, C., Compo, G.P., 1998. A practical guide to wavelet analysis. Bulletin of the
981 American Meteorological Society. 79, 61–78. doi:10.1175/1520-
982 0477(1998)079<0061:APGTWA>2.0.CO;2

983 Tucker, C.J., 1979. Red and photographic infrared linear combinations for monitoring
984 vegetation. Remote Sensing of Environment. 8, 127–150. doi:10.1016/0034-
985 4257(79)90013-0

U.S. Geological Survey, 2018a. Product Guide: LANDSAT 4-7 SURFACE REFLECTANCE (LEDAPS) PRODUCT. Department of the Interior Version 8.3, https://landsat.usgs.gov/sites/default/files/documents/ledaps_product_guide.pdf (accessed 03 January 2018)

U.S. Geological Survey, 2018b. Product Guide: Landsat 8 Surface Reflectance code (LaSRC) product. Department of the Interior Version 4.3, https://landsat.usgs.gov/sites/default/files/documents/lasrc_product_guide.pdf (accessed 03 January 2018)

Velloso, A. L., Sampaio, E. V. S. B., Pareyn, F. G. C, 2001. Ecorregiões: propostas para o bioma caatinga; resultados do seminário de planejamento ecorregional da caatinga. Seminário de Planejamento Ecorregional da Caatinga. TNC/APNE Recife, Aldeia-Pernambuco, 76.

Verbesselt, J., Hyndman, R., Newnham, G., Culvenor, D., 2010. Detecting trend and seasonal changes in satellite image time series. Remote Sensing of Environment. 114, 106-115. doi:10.1016/j.rse.2009.08.014

Verbesselt, J., Umlauf, N., Hirota, M., Holmgren, M., Van Nes, E.H., Herold, M., Zeileis, A., Scheffer, M., 2016. Remotely sensed resilience of tropical forests. Nature Clima Change. 6, 1028-1031. doi:10.1038/nclimate3108

Verbesselt, J., Zeileis, A., Herold, M., 2012. Near real-time disturbance detection using satellite image time series. Remote Sensing of Environment. 123, 98-108. doi:10.1016/j.rse.2012.02.022

Vermote, E., Justice, C., Claverie, M., Franch, B., 2016. Preliminary analysis of the performance of the Landsat 8 / OLI land surface reflectance product. Remote Sensing of Environment. 185, 46-56 doi:10.1016/j.rse.2016.04.008

Vicente-Serrano S.M., Beguería, S. López-Moreno, J.I., 2010. A Multi-scalar drought index sensitive to global warming: The Standardized Precipitation Evapotranspiration Index - SPEI. Journal of Climate 23, 1696-1718. https://doi.org/10.1175/2009JCLI2909.1

Walker, J., de Beurs, K., Wynne, R.H., 2015. Phenological response of an Arizona dryland forest to short-term climatic extremes. Remote Sensing 7, 10832–10855. doi:10.3390/rs70810832

Wang, Z., Erb, A.M., Schaaf, C.B., Sun, Q., Liu, Y., Yang, Y., Shuai, Y., Casey, K.A., Román, M.O., 2016. Remote Sensing of Environment Early spring post- fi re snow albedo dynamics in high latitude boreal forests using Landsat-8 OLI data. Remote Sensing of Environment. 185, 71–83. doi: 10.1016/j.rse.2016.02.059

Wang, Z., Schaaf, C.B., Sun, Q., Kim, J., Erb, A.M., Gao, F., Román, M.O., Yang, Y., Petroy, S., Taylor, J.R., Masek, J.G., Morisette, J.T., Zhang, X., Papuga, S.A., 2017. Monitoring land surface albedo and vegetation dynamics using high spatial and temporal resolution synthetic time series from Landsat and the MODIS BRDF/NBAR/albedo product. International Journal of Applied Earth Observation and Geoinformation. 59, 104-117 doi:10.1016/j.jag.2017.03.008

Wessels, K.J., Prince, S.D., Malherbe, J., Small, J., Frost, P.E., VanZyl, D., 2007. Can human-induced land degradation be distinguished from the effects of rainfall variability? A case study in South Africa. Journal of Arid Environment. 68, 271–297. doi:10.1016/j.jaridenv.2006.05.015

Wessels, K.J., Van den Bergh, F., Scholes, R.J., 2012. Limits to detectability of land degradation by trend analysis of vegetation index data. Remote Sensing of Environment. 125, 10–22. doi:10.1016/j.rse.2012.06.022

Wulder, M.A., White, J.C., Loveland, T.R., Woodcock, C.E., Belward, A.S., Cohen, W.B., Fosnight, E.A., Shaw, J., Masek, J.G., Roy, D.P., 2016. The global Landsat archive: Status, consolidation, and direction. Remote Sensing of Environment. 185, 271–283. doi:10.1016/j.rse.2015.11.032

Xu, D., Guo, X., Li, Z., Yang, X., Yin, H., 2014. Remote Sensing of Environment Measuring the dead component of mixed grassland with Landsat imagery. Remote Sensing of Environment. 142, 33–43. doi:10.1016/j.rse.2013.11.017

Yang, Y., Wang, Z., Li, J., Gang, C., Zhang, Y., Zhang, Y., Odeh, I., Qi, J., 2016. Comparative assessment of grassland degradation dynamics in response to climate variation and human activities in China, Mongolia, Pakistan and Uzbekistan from 2000 to 2013. Journal of Arid Environments. 135, 164–172. doi:10.1016/j.jaridenv.2016.09.004

Yu, Y., Notaro, M., Wang, F., Mao, J., Shi, X., Wei, Y., 2017. Observed positive vegetation-rainfall feedbacks in the Sahel dominated by a moisture recycling mechanism. Nature Communications. 8, 1–9. doi:10.1038/s41467-017-02021-1

Zeileis, A., Leisch, F., Hornik, K., Kleiber, C., 2002. strucchange : An R Package for Testing for Structural Change in Linear Regression Models 1–38. Available in: https://cran.r-project.org/web/packages/strucchange/vignettes/strucchange-intro.pdf

Zhang, J., Niu, J.M., Bao, T., Buyantuyev, A., Zhang, Q., Dong, J.J., Zhang, X.F., 2014. Human induced dryland degradation in Ordos Plateau, China, revealed by multilevel statistical modeling of normalized difference vegetation index and rainfall time-series. Journal of Arid Land 6, 219–229. doi:10.1007/s40333-013-0203-x

Zhao, Y., Wang, X., Novillo, C.J., Arrogante-Funes, P., Vázquez-Jiménez, R., Maestre, F.T., 2018. Albedo estimated from remote sensing correlates with ecosystem multifunctionality in global drylands. Journal of Arid Environments. 157, 116–123. doi:10.1016/j.jaridenv.2018.05.010

LIST OF FIGURE CAPTIONS

Fig. 1 - (A) Location of the Caatinga forest, Landsat scene 215/065 (path/row) and study area (Xmin: 37.07ºW; Xmax: 36.84ºW; Ymin: 7.86ºS; Ymax: 7.74ºS, WGS 84); (B) Landsat 5 false colour composite (RGB to bands 4, 3 and 2) of the study area on 17/06/1984; (C) Landsat 8 false colour composite (RGB to bands 5, 4 and 3) of the same area of (B) on 06/05/2015, showing land-cover differences between the first and last years of the studied period.

Fig. 2 - The 12-month Standardized Precipitation-Evapotranspiration Index - SPEI 12 (source: Beguería et al., 2017) and CHIRPS Precipitation (source: Funk et al., 2015) at geographic coordinates 36.75º W, 7.75º S (WGS 84).

Fig. 3 - Location of the validation sites in the study area: 45 target areas (numbered, 31 target areas where a LCC actually occurred and 14 areas with preserved natural vegetation), the Subset I that had a sequential land-cover clearing process during 2003–2012 and the Subset II validation area. Source: Landsat 8 false colour composite (RGB to bands 5, 4 and 3).

Fig. 4: TSS-RESTREND structural change detection outputs for the target area 22. Top row panel shows SA, EVI and NDVI entire time series data, whereas the next panel has complete OPA time

1077 series, followed by monthly residuals of OPA, and Trend to each time series spectral indices. In the
1078 Trend panel, vertical lines represent breakpoints and the bold vertical line the most significant
1079 breakpoint.

1080 Fig. 5 – Detected and actual year of land-cover clearing for SA, EVI and NDVI for the 45 target areas:
1081 A) Description and B) Summary

1082 Fig. 6 – Polygon (subset I) with patches showing the detected breakpoint years of LCC for SA, EVI,
1083 NDVI and actual LCC year.

1084 Fig. 7 - Observed change year LCC for the patches compared with the results of TSS-RESTREND for
1085 SA, NDVI and EVI: A) percentage of pixels in each patch classified as false negative; B) median of the
1086 detected LCC for all pixels within a patch. The dotted line is the 1:1 line and τ is the Kendall rank
1087 correlation coefficient.

1088 Fig. 8 – Barplots of the detected LCC year obtained by TSS-RESTREND for the three spectral indices
1089 (SA, EVI and NDVI) for the patches of the Subset I region. The height of each black bar is the
1090 percentage of pixels where a change was detected in that year. Red bars correspond to pixels where
1091 no change was detected. Grey dashed lines show observed LCC years.

1092 Fig. 9 - Detected LCC year by the TSS-RESTREND based on SA time series for the Subset II
1093 highlighted in Fig. 3. Image source: Landsat 5 (RGB to 4, 3 and 2) and Landsat 8 (RGB to 5, 4 and 3)
1094 false colour composite.